Developments in the Built Environment 20 (2024) 100566

Contents lists available at ScienceDirect

Developments in the Built Environment

journal homepage: www.sciencedirect.com/journal/developments-in-the-built-environment

Urban heat islands' effects on the thermo-energy performance of buildings according to their socio-economic factors

Rafael E. López-Guerrero [a,b], Konstantin Verichev [c], Juan Pablo Cárdenas-Ramírez [d], Manuel Carpio [b,e,f,*]

[a] Departamento de Ciencias de la Construcción, Universidad del Bio-Bio, Concepción, Chile
[b] Department of Construction Engineering and Management, School of Engineering, Pontificia Universidad Católica de Chile, Santiago, Chile
[c] Instituto de Obras Civiles, Universidad Austral de Chile, Valdivia, Chile
[d] Universidad Autónoma de Chile, Facultad de Arquitectura, Construcción y Medio Ambiente, Temuco, Chile
[e] Centro Nacional de Excelencia para la Industria de la Madera (CENAMAD), Pontificia Universidad Católica de Chile, Santiago, Chile
[f] Department of Construction Engineering and Project Management, University of Granada, Spain

ARTICLE INFO

Keywords:
Urban heat island
Housing models
Thermo-energy performance
Socio-economic contrasting districts
Sustainability

ABSTRACT

Urban areas experience the urban heat island (UHI) effect, which affects the thermal comfort and energy consumption of buildings. These consequences could vary depending on the socio-economic status of the neighbourhoods. Few studies have investigated how UHI affects socio-economically contrasting districts in thermal comfort and energy performance. Therefore, the primary goal of this research is to evaluate and compare the energy efficiency and thermal comfort conditions of residential buildings in the same city (Temuco, Chile) but located in socio-economically contrasting neighbourhoods. Urban weather files were first modelled in four urban zones using UWG software. Also, EnergyPlus building simulations were conducted to evaluate discomfort hours in adaptive comfort models and energy performance. The results showed annual average UHI intensities between 1.5 and 2.5 K. Urban–rural cooling energy load differences ranged between 12.47% and 38.92%, while heating energy load differences ranged between −20.47% and −81.95%. These distinctions depended on the urban zone, residence model analysed, or energy building standard applied. Similarly, urban-rural differences in thermal comfort times varied from 0.5% to 100%. Results illustrate that the risk of overheating could increase in socio-economically vulnerable areas. This issue could worsen if urban segregation continues to generate poor urban design in low-income districts.

1. Introduction

Addressing the intertwined issues of climate change and sustainable development requires a focus on cities as key drivers of global transformation (Bazaz et al., 2018; UN). Also, more than half of the world's population currently resides in urban areas, a number projected to increase to 68% by 2050 (ONU, 2018). This trend is particularly pronounced in regions like Latin America and the Caribbean, where urban populations are already at 80.7% and are expected to reach 87.8% by 2050 (ONU, 2018), (Roy et al., 2018).

Buildings account for 35% of global energy consumption and 38% of greenhouse gas emissions (UNEP, 2020). However, achieving energy efficiency in buildings requires an understanding of urban climatic variables, which are quite relevant to transforming the weather of microclimates (Oke, 1995). Urban climates could differ significantly from rural ones and, consequently, might have an important gap between urban weather files and those performed at rural meteorological stations, which are typically used for energy design simulations (Palme et al., 2017), (Salvati et al., 2019). This phenomenon is produced by the urban heat island (UHI) effect, which is basically described as elevated temperatures in urban areas compared to surrounding rural areas (Oke et al., 2017).

The UHI effect is among the key challenges in urban environments. It is influenced by various factors, including land use changes, building materials, urban morphology and anthropogenic heat generation (Hong et al., 2020), (Woong Kim and Brown, 2021) The UHI is associated with

* Corresponding author. Department of Construction Engineering and Management, School of Engineering, Pontificia Universidad Católica de Chile, Santiago, Chile.

E-mail addresses: manuel.carpio@uc.cl, carpio@ugr.es (M. Carpio).

https://doi.org/10.1016/j.dibe.2024.100566
Received 3 January 2024; Received in revised form 4 September 2024; Accepted 24 October 2024
Available online 4 November 2024
2666-1659/

various socio-environmental and economic impacts, including an increase in photochemical smog and urban pollution (Ulpiani, 2021), (Li et al., 2018) an increase in morbidity and mortality due to air pollution or intensifying heat waves (Gholizadeh Touchaei, 2015), (Santamouris and Fiorito, 2021), (Chen et al., 2014) in thermal comfort conditions (Giridharan and Emmanuel, 2018), (He et al., 2020) energy consumption for building air conditioning (Palme et al., 2017), (Boccalatte et al., 2020) among other effects. Thus, understanding the thermal performance of buildings within urban environments is critical for designing energy-efficient and sustainable solutions.

Likewise, cities experience other issues regarding global sustainability. Most worldwide cities are characterised by several inequalities in the distribution of their commons, including, for example balanced land use, green areas, urban water bodies etc. (Kato-Huerta and Geneletti, 2022), (Kim et al., 2022), (Han et al., 2023), (Tammaru et al., 2020). Low-income districts usually lack basic services and amenities, which worsens their socio-economic conditions, becoming a vicious circle that hinders their complete development (Kim et al., 2022), (Tammaru et al., 2020), (Fernández et al., 2023), (Feitosa et al., 2023), (Zhang et al., 2021). Thus, the evaluation of socio-economically vulnerable districts is also fundamental to achieving holistic sustainability and the development of urban spaces (Roy et al., 2018), (Tammaru et al., 2020), (Fernández et al., 2023).

Some of the main problems in these vulnerable urban areas are related to either denser urban areas or urban vegetation scarcity, which are some of the main triggers of UHI phenomena (Oke, 1995), (Lindberg and Grimmond, 2011), (Koch et al., 2020). Considering this context, UHI influences over buildings could be greater in socio-economically unprivileged structures in less wealthy urban areas, once there is an inverse relationship between socio-economic conditions and the probability of UHI, as stated in recent research (Eugenio Pappalardo et al., 2023), (Sarricolea et al., 2022). Moreover, socio-economic inequalities are one of the main problems in Latin American cities, which have been expanded under poorer urban model developments dominated by social segregation and real estate speculation (UN-HABITAT, 2012), (Henríquez and Romero, 2019), (CEPAL, 2017). In this regard, some studies have demonstrated the relationship between urban inequalities and the possible formation of UHI in South America (Sarricolea et al., 2022), (Montaner-Fernández et al., 2020), (Sarricolea and Meseguer-Ruiz, 2019), (da Silva et al., 2023a). This problem affects not only developing countries but also developed ones (Chakraborty et al., 2019), (Venter et al., 2023). However, the study of this topic has become especially important in urban districts with lower socio-economic settings or even in countries that suffer from energy poverty conditions (Calvo et al., 2021).

Energy poverty has emerged in recent decades as an important phenomenon and worldwide research field (Guevara et al., 2023), which refers to a condition in which individuals or households have limited access to affordable, reliable and modern energy services that are essential for meeting their basic needs and improving their quality of life (Culver, 2017). One of the most important deficiencies in energy poverty is the capacity to warrant comfortable indoor environmental conditions, either in the summer or winter, using a passive mode or mechanical systems (Calvo et al., 2021). However, some low-income populations globally cannot afford to ensure year-round comfortable conditions. This is the case, for example, in several countries in Latin America, Africa and Asia, where low-income communities tend to prioritise and invest in better residential indoor conditions during prevailing heating seasons (in higher latitudes or altitudes) and neglect their comfort in the summer (Calvo et al., 2021), (Chan and Delina, 2023), (IEA), (Mastrucci et al., 2019). Furthermore, according to the historically predominant local climate, residential housing could not be well designed to maintain comfortable conditions during one season as opposed to another (IEA), (Matos et al., 2022), (Verichev and Carpio, 2020).

Regarding the impact of UHI on energy building performance, a vast number of studies have been conducted to demonstrate overheating issues due to higher urban temperatures produced either by UHI or the global warming effect, (Li et al., 2019), (Santamouris, 2014), (Santamouris et al., 2015). In this regard, the difference between urban and rural building performance was reported as a 23.2% average increase in cooling energy consumption and an 18% decrease in heating energy consumption (López-Guerrero et al., 2022), (Li et al., 2019). Similarly, the cooling penalty due to the increase in one degree of temperature or UHI intensity (UHII) by a surface building for residential use was reported at 6.63 kWh/m^2/year/K, which is the building use more affected (Lopez-Guerrero et al., 2023).

Nonetheless, there is a scarcity of studies assessing how UHI affects the thermo-energy performance of buildings according to their socio-economic status or possible energy poverty, as demonstrated by (López-Guerrero et al., 2022). In addition, according to the authors, there are few studies focused on UHI effects considering the impact on urban buildings in passive mode, which means without HVAC systems during summer seasons. Thus, there is also a shortage of research on UHI effects over indoor thermal comfort conditions, considering how different residential thermal zones (daytime- or nighttime-occupied) are affected depending on the thermal and socio-economic capacity of different districts.

Therefore, the central question of this research is: how do different urban zones, particularly residential buildings, experience the UHI effect in relation to their socio-economic status? Answering this question could be especially relevant in countries where heating seasons have been prioritized in public policies due to historically predominant local climates. This is the case, for example in southern Latin America. Thus, the main objective of this research is to assess and compare the building energy performance and thermal comfort conditions of residential buildings in the same city but placed in contrasting socio-economic neighbourhoods. The buildings assessed are also influenced by the UHI effect and are characterised by different building thermal properties according to their socio-economic status. The study focused on Temuco city, a southern Chilean city where heating comfort conditions have generally been privileged. For this, the urban tissue was also analysed to understand how chances in urbanisation parameters could similarly influence the formation of UHI and consequently affect the environmental performance of residential districts in different ways.

2. Methodology

This research evaluated the thermo-energy performance of four types of single-family residences in different morphological and socio-economic districts of the same city. First, the case study city was divided and characterised in detail in homogeneous zones, according to each morphological and metabolic condition. Then, according to these conditions, four weather data files from the four main predominant urban zones were modelled to include the UHI effect. The case study city was also mapped, agreeing with socio-economic conditions. Out of the four residential models, three were developed based on houses that represent real conditions and the characteristics of two contrasting socio-economic statuses. Specifically, the two models reflect a low-income district, while the other represents a medium-high-income area. The fourth model represents a typical residential apartment in medium-income districts. These four models were then simulated in their respective socio-economic neighbourhoods. However, every model was hypothetically simulated in the remaining three microclimatic urban zones and also with the reference rural weather data file, totalling five simulations for every residential model. From these 20 simulation cases, building energy loads and overheating discomfort conditions were evaluated from three adaptive comfort models. The thermal comfort performance was also analysed separately between thermal zones occupied in the daytime or nighttime. Finally, a sensitivity analysis (SA) was conducted to better understand the parameters that affect summer season thermo-energy building performance in naturally ventilated residential models under the UHI effect. The SA was conducted in only two model houses that comply with the recently updated national energy standard. Before these processes, indoor and outdoor field measurements were performed to compare them with the simulation models. In addition, certain ground thermal parameters were measured in the field to reduce uncertainty in the simulation process. The entire methodological process is also described in Fig. 1, Table 1. The following sections will provide a more detailed explanation of each methodological step in the research.

2.1. Case study

Temuco city serves as the capital of the Araucanía Region in southern Chile (longitude 38.76°E; latitude 72.63°S). As per official population projections, Temuco stands as a medium-sized city boasting a population of 308,175 inhabitants (INEa). The city is characterised by mild and temperate summers, along with rainy winters. The average annual temperature was 11.4 °C, with an approximate precipitation of 1482 mm. Furthermore, it falls under the Mediterranean-type climate or Csb classification according to the Köppen–Geiger climate classification (Peel et al., 2007; Climate data), with warm and dry summers and mild and wet winters.

2.1.1. Socioeconomic and urban characteristics

This research analyzes the influence of the UHI effect on the thermo-energy performance of residential buildings across different socioeconomic contexts and urban fabrics. Accordingly, this study selected two socio-economic districts in Temuco city. In Chile, the population and residential units are further delineated by their socio-economic strata and partitioned into five tiers, ranging from the most modest to the most affluent: D-E-C1-C2-ABC1 (INEa). Among the two selected areas, the Pueblo Nuevo District represents a low-income neighbourhood (levels D and E), hereafter termed L_D. The Villa Tobalaba District represents the medium-high-income segment (levels C2 and ABC1), hereafter called M_D (Fig. 2). These areas were chosen due to their similar housing conditions and predominant house types (single-family and semi-detached one-story structures). Additionally, both neighbourhoods share the same founding era (1980s) and similar elevations (141 and 132 m above sea level for L_D and M_D, respectively). Despite their shared founding era, M_D has updated its construction characteristics to meet the new energy standards mandated in Temuco, namely, the Plan for Atmospheric Decontamination (PDA in its Spanish acronym; MMA, 2015), whereas L_D has made minimal progress in this regard (INEc).

It is important to emphasize that these disparities shape the characteristics of each district, as populations construct their buildings according to their own socioeconomic capacity. However, although L_D has fewer buildings adapted to the newer code, the prevailing cold weather conditions is driving the need for retrofitting, often supported by government financial programs (MMA). Additionally, L_D faces challenges such as lower levels of urban vegetation and higher building density, conditions commonly found in vulnerable neighbourhoods. These factors might be associated with urban speculation and gentrification, phenomena encountered in Temuco city (Rojo-Mendoza et al., 2019). Vegetated areas are significantly reduced in L_D compared to those in higher socioeconomic areas of Temuco, either due to the absence of urban parks or streets with little to no vegetation. As a result, they contribute to a particular urban fabric that tends to intensify the UHI effect over residential buildings (Sarricolea et al., 2022).

2.2. Urban classification

To evaluate the urban tissue for energy building proposals, some urban classification methods have been proposed, such as urban tissue categories (Palme et al., 2017) or Local Climates Zones (LCZ) (Stewart and Oke, 2012). In this research, LCZ classification was selected for urban analysis. The LCZ classification introduces 17 local climate zones, 10 of which delineate urban areas based on their density, urban vegetation, soil permeability and other surface properties (Stewart and Oke, 2012). This classification method has been employed as a foundational framework for global analysis and plays a pivotal role in standardising methodologies for assessing UHI impacts worldwide (Yang et al., 2020), (Martilli et al., 2020), (Aslam and Rana, 2022).

This research conducted LCZ mapping through two approaches: manual mapping and enhanced utilisation of the World Urban Database and Portal Tool (WUDAPT), in conjunction with Landsat satellite imagery (Bechtel et al., 2019), (Bechtel et al., 2015). In the case of manual mapping, a data collection campaign was undertaken. LCZ classification necessitates the consideration of 10 urban parameters that collectively determine each LCZ class (Stewart and Oke, 2012). Among these, the sky

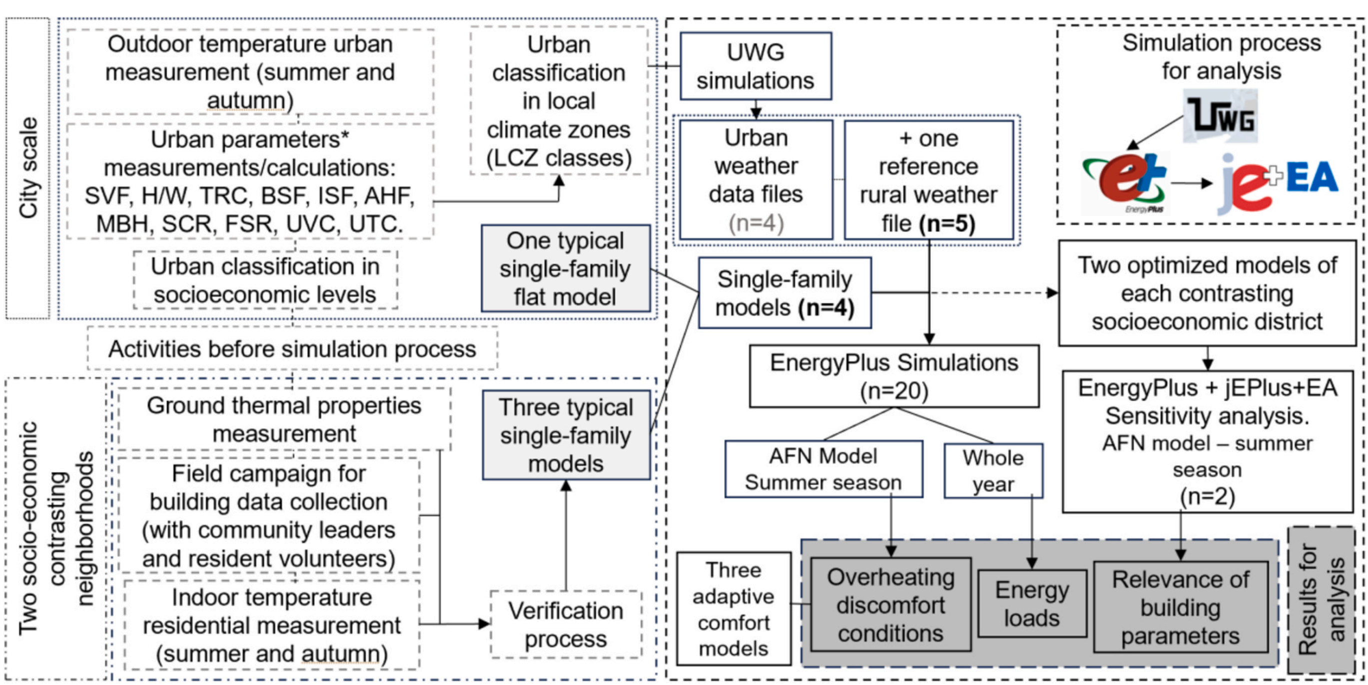

Fig. 1. Research methodological scheme. AFN: Airflow network model of EnergyPlus software. (*) For acronyms' interpretation, see Table 2.

Table 1
Simulation model description.

Name of model	L_OGUC / L_PDA	M_PDA	M_FLAT
Corresponding district	L_D	M_D	M_D
Energy standards	OGUC / PDA with updated OGUC and Standard for Sustainable Building	PDA with updated OGUC and Standard for Sustainable Building	PDA with updated OGUC and Standard of Sustainable Building
Residential type	Semidetached Low-income model	Semidetached medium-income model	Medium-income department
Typical socio-economic level	Low (C1, E, D)	Medium-High (ABC1–C2)	Medium (C2)
3D image	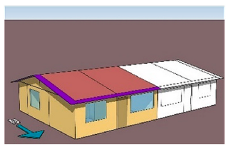	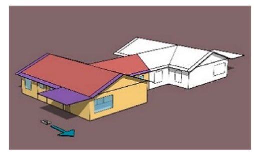	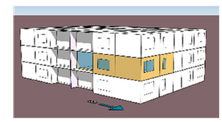
Main plan		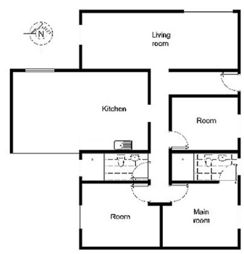	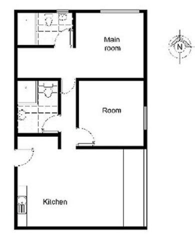
Surface (m^2)	59.5	108	71.5
Indoor high (m)	2.4	2.4	2.4
Wall material	Wood	Wood/Concrete	Concrete
Floor material	Wood	Wood/Concrete	Wood/Concrete (adiabatic)
Roof material	Zinc/wood	Zinc/wood	Concrete (adiabatic)

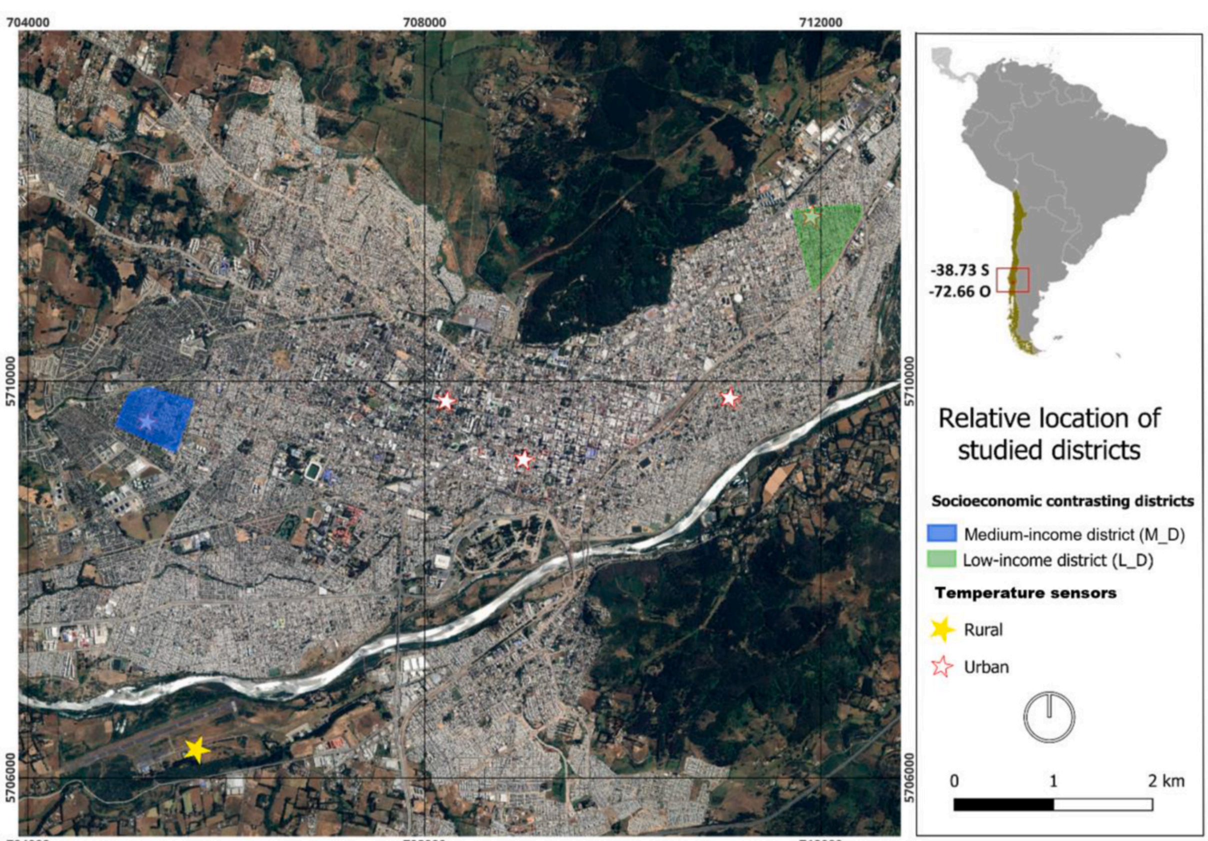

Fig. 2. Temuco city's contrasting localisation and socio-economic districts were studied.

view factor was estimated through fisheye lens photography of representative streets within each urban region, followed by image processing using the RayMan software algorithm (Matzarakis et al., 2006). Similarly, the Canyon aspect ratio was determined by sampling typical streets during field campaigns. The mean building height was extracted from the local urban database (Temuco, 2015) and cross-referenced with Google Street View. The Terrain roughness class was established based on the Davenport classification (Davenport G et al., 2000). The building surface fraction, impervious surface fraction and pervious surface fraction were derived from the analysis of the normalized difference built-up index (NDBI), normalized difference vegetation index (NDVI), data from Landsat 8 and Sentinel high-resolution satellite images and CAD mapping available within the local database (Temuco, 2015). For this study, the calculation of surface admittance, albedo and anthropogenic heat flux from sources other than vehicular traffic was omitted due to a dearth of data specific to the study area.

Anthropogenic heat flux (AHF) originating from vehicular traffic is considered a relevant parameter in UHI formation, as it can contribute up to 30% of heat in some urban centres (Wagner and Viswanathan, 2016). In this work, AHF sources were computed using a previously proposed methodology (Quah and Roth, 2012), (Grimmond, 1992). Thus, an official local database was utilised (SECTRA) that included regular traffic volume data collected at various urban locations and time intervals. Thus, the hourly heat emission resulting from the combustion of vehicle fuels, denoted QV (h), was calculated according to eqs. (1) and (2) (Quah and Roth, 2012), (Grimmond, 1992)

$$Qv(h) = \left[\sum_{ijk} \left(n_{vijk}\ (h) \times EV_{ij} \times d_k \right) \ / \ 3600 \right] \Big/ A \ \left[W\, m^{-2} \right] \tag{1}$$

$$EV_{ij} = \left(NHC_j \times \rho_j \right) \ / \ FE_{ij} \ \left[\mathrm{J}\, m^{-1} \right] \tag{2}$$

where h represents the local time in hours. Subscripts i, j and k denote the vehicle class, fuel type and road segment, respectively. For the remaining values, the authors refer the reader to (Quah and Roth, 2012), (Grimmond, 1992).

2.3. UHI modelling

To estimate urban weather data, this study employed the open-access Urban Weather Generator V 4.1 (UWG) tool (Bueno et al., 2013). The reliability of this software has been established through extensive use and validation by prior researchers (Salvati et al., 2019), (Bueno et al., 2014), (Mao et al., 2017). The inputs required by UWG are categorised into microclimate parameters, urban characteristics, vegetation parameters and building surfaces and typologies. Notably, the most influential input parameters have been identified in earlier studies (Salvati et al., 2019), (Nakano et al., 2015) and are typically computed for the most representative urban regions. Among these, key parameters include the average building height, site coverage ratio and façade-to-site ratio. These parameters were estimated manually using the same techniques detailed in Section 2.2, relying on official local data and high-resolution satellite images (Temuco, 2015). Similarly, metrics were adapted such as urban area vegetation coverage, urban area vegetation trees and sensible anthropogenic heat. Anthropogenic heat originating from vehicular traffic was computed, as stated in Section 2.2. Building surfaces were quantified using high-resolution satellite images and computer-aided drafting (CAD) urban maps derived from local research (Temuco, 2015). Thermal building attributes were tailored to adhere to Chilean local standards (see Table 1) for the corresponding building climate zone of Temuco city (Zone 5) (Ministerio de Vivienda y Urbanismo, 1999). Notably, residential cooling demands within Temuco city are notably low (CDT, 2019), and most residences are naturally ventilated during summer. Therefore, in UWG, cooling setpoints were established at 35 °C for the entire day for the residential LCZ class. Finally, for all LCZ classes, the simulation was run for 365 days.

2.4. Building models

In this research, two typical semidetached houses in Temuco city were selected (Table 1). A typical residential flat was also analysed. These models were chosen according to the socio-economic district where they typically stand (INE, 2017a) and the current Chilean building energy-thermal standards. It is pertinent to emphasize that the studied low-income district (L_D) predominantly comprises houses adhering to a current mandatory national thermal standard, namely the General Urban Planning and Construction Ordinance (OGUC by its Spanish acronym; (Ministerio de Vivienda y Urbanismo, 1999). This standard is relatively lenient. However, as beforementioned, since 2015, PDA has been introduced (MMA, 2015). In addition, building parameters in the OGUC standard have recently been updated to align with those proposed in the PDA, although these changes will not take effect until 2025 (MINVU, 2024). Therefore, the model house simulated in L_D is subdivided into two types, namely one with the OGUC standard (L_OGUC model) and one with the PDA standard (L_PDA), both with the same layout (Table 1). Thus, although L_PDA represents a lower proportion compared to L_OGUC (INEa), both models were used in this research for in-depth analysis. However, the PDA standard has been more widely embraced in M_D (M_PDA). Therefore, the L_PDA, M_PDA, and M_FLAT models were configured using PDA standard. Additionally, the Sustainable Building Standard proposed in 2018 (MINVU, 2018a) was also considered. In this context, four residential buildings were simulated (Table 1). All building simulations were carried out with EnergyPlus software V22.2 (Crawley et al., 2001) for an entire year. The simulation parameters are described in Appendix A.

In addition, it is important to highlight that simulation models for natural ventilation during summer to evaluate comfort performance were conducted using the Airflow Network (AFN) model of EnergyPlus software. The AFN model offers the capability to simulate wind-driven airflows across multiple zones (EnergyPlus). Here, *natural ventilation* refers to airflow resulting from open or partially open exterior windows and doors. This also allows the zone level to be set to control natural ventilation, defining windows/door with a component-opening object and set points that control the opening of windows and doors in the thermal zone. For detailed information about AFN, the authors refer the reader to Choi et al. (2023) and (EnergyPlus). AFN simulations were performed for the summer season (from December to March in the Southern Hemisphere). Appendix A presents the main simulation inputs for the AFN model.

2.5. Building model verification

To verify the reliance of models, three sample houses were selected, and three processes were conducted in real and simulated models: (i) relevant values for ground temperature heat transfer were measured and adjusted in simulation models; (ii) heating loads were calculated in real sample houses and simulated ones; and (iii) indoor temperature measurements were made in two thermal zones in both residential districts (L_D and M_D) during the summer (and autumn) season, after which results were compared with the same simulated models as naturally ventilated spaces. Due to the important influence of the infiltration rate in heating energy performance (Laverge and Janssens, 2013), in this study, this parameter was adjusted for verification procedures based on the methodology used by Aparicio-Fernández et al. (2019). In this process, infiltration rates were slightly adapted (see Appendix A) to obtain similar heating loads between the models and real houses monitored. This adjustment was also made to achieve indoor air temperatures similar to those monitored in the summer season (without a cooling system). The methods used in every step are described in the following sections.

2.5.1. Ground temperatures

Field measurements were conducted to determine the relevant value parameters, recognising the substantial impact of ground temperature on building simulation calibration (González et al., 2022) and considering the different models used in EnergyPlus software to characterise the thermal interaction of the model with the ground. Thus, in-situ measurement discerned the thermal conductivity, density and moisture content of soil within the two districts with contrasting socio-economic levels (L_D and M_D in Table 1). The KD2 Pro Thermal Properties Analyzer, Model TR-1, was employed to measure thermal conductivity, while the method of hydrostatic balance proposed by (Asociación Española de Normalización y Certificación, 1994) was utilised for density and moisture content calculations. This method was conducted in the Materials Laboratory of the University of the Frontier (Temuco, Chile) after soil sample collection in the field. Therefore, after data were obtained, the optimised Finite Difference Model was employed within EnergyPlus to calculate ground temperatures, once it was one of the more accurate models to perform ground temperature calculations (González et al., 2022).

2.5.2. Heating load comparison

According to national statistics, Temuco city heavily depends on firewood, with approximately 79.47% of households relying on it as their primary heating fuel during winter (Reyes et al., 2020). Additionally, the utilisation of electricity for cooling purposes is very scarce (CDT, 2019). Therefore, in this research, a simple verification of the models was approached through an analysis of energy loads' firewood and/or pellet consumption during the heating season. Subsequently, the results were compared with simulation outcomes during a heating season. Importantly, as beforementioned, for this verification process, infiltration rates were adjusted to obtain a similar heating performance. Verification was conducted in the L_OGUC, L_PDA and M_PDA models (Table 1).

For this task, neighbourhood council chiefs and dwelling owners were consulted through field verification to ascertain the quantities of average annual wood and/or pellet consumed by each studied district and house (L_D and M_D). Next, the methodology outlined by Reyes et al. (2020) was employed to calculate the performance of energy loads (Reyes et al., 2020), considering the average firewood and/or pellet consumption obtained from the survey.

2.5.3. Indoor temperature comparison

Measurements of indoor air temperature were conducted in both contrasting socio-economic districts (L_D and M_D); the method used is better explained in Section 2.6. After the synchronised adjustment of infiltration rates and heating loads, the simulation results were compared with air temperature measurements. To compare the accuracy of simulation models for energy building purposes, several indexes have been proposed, as described in ASHRAE Guideline 14–2014 (ASHRAE, 2014). In this research, normalized mean bias error (NMBE) and coefficient of variation of the root mean square error, or CV(RMSE), were used to verify the models. CV(RMSE) offers insights into the proximity of simulation predictions to actual data, whereas NMBE functions as a gauge for the overall bias present in the simulation predictions (Chong et al., 2021, eqs. (3) and (4)):

$$\text{NMBE}\ (\%) = \frac{1}{\overline{m}}\ x \frac{\left(\sum_{i=1}^{n} (m_i - s_i)\right)}{n - p}\ x\ 100 \quad (3)$$

$$\text{CV(RMSE)} = \frac{1}{\overline{m}} \sqrt{\frac{\sum_{i=1}^{n} (m_i - s_i)^2}{n - p}}\ x\ 100 \quad (4)$$

where m_i is measured data, s_i is simulated data, $\overline{m}$ is the mean of the measured data, n is the number of data points, and p is the number of adjustable model variables.

2.6. Field temperature measurements

Considering local UHI estimations, it is important to obtain data from field measurements to compare every urban area mapped in the LCZ scheme and modelled in the UWG. For this, several sensor temperatures (°C) were installed in the studied area. Thus, six sensors (Model HOBO MX 2302A) with an accuracy of ± 0.2 °C and ± 2.5% were installed in the most representative LCZ in the studied city. According to Stewart and Oke (2012), the typical circle of influence of every sensor has a radius of 200–500 m (Stewart and Oke, 2012). Thus, one sensor was installed for each zone. The sensors were installed 2 m above ground, far from any artificial heat source, at least 2.5 m from any obstacle (roofs and walls) (Oke, 2006) (See Table 2). Similarly, another datalogger was installed in a rural area in the southeast, 8 km (straight line) from the city centre. Moreover, rural weather data were obtained from the Maquehue meteorological station (Meteochile), which is located in the southwest, 5 km from the city centre (straight line; Fig. 2).

In addition, indoor measurements were conducted in the two socio-economic residential districts (Fig. 1) for the verification process (Section 2.5.3). Considering that the M_D and the L_D are characterised by predominant semi-detached single-family houses (Table 1), one representative house of each district was selected for monitoring. For this, Netatmo indoor weather stations (Netatmo) were installed to measure indoor and outdoor temperatures (°C). The accuracy of stations is ± 0.3 C° (Alonso et al., 2022). The indoor measurements were taken in the living space, main bedroom and outdoors of every sample house in every socio-economic district during summer and autumn (December 2021 to June 2022).

Three semidetached houses were selected for indoor measurements, each one representing Chilean thermal building standards, namely L_OGUC, L_PDA and M_PDA (Table 1). Other criteria were used to select these houses; in the case of L_OGUC, this should have preserved its original envelope characteristics, without any refurbishment or adaptation to the new standard (PDA). In addition, L_OGUC should have built wood envelopes into external walls, which represents 42.24% of the housing stock and is the most representative building material in Temuco (INEc). In the case of L_PDA and M_PDA, these should have been adapted to the new regional standard (PDA) in the building envelope (e.g. double-glazing windows and wider insulation panel). For all models, the roof envelope material should have been built with zinc plates and wooden flooring material, which represents 71.51% and 82.3% of Temuco housing stock, respectively (INEc). Similarly, all houses should have been constantly inhabited by at least three persons, which is the average number stated in the last regional census (INEb).

2.7. Comfort models

One of the main purposes of this research was to assess how the UHI effect influences the comfortability of residential buildings during summer. Hence, three adaptive comfort models for naturally ventilated buildings were used. Adaptive comfort models play a pivotal role in establishing standards for comfort when evaluating building comfort in free-running mode. These models acknowledge that occupants can adjust to the thermal environment around them through behavioural, physiological and psychological responses (Pérez-Fargallo et al., 2018).

Currently, there is a scarcity of adaptive comfort models developed specifically for Chilean purposes (Pérez-Fargallo et al., 2018). Consequently, this research considered three models to evaluate the risk of overheating due to the UHI effect in Temuco. The models used were (i) CIBSE TM52 (CIBSE, 2013), (ii) ASRHAE 55 (2010) (ASHRAE, 2010) and (iii) Dear and Brager Comfort Model (De Dear and Brager, 1997). The latter was used because it is the only comfort model considered in the Sustainable Construction Standard for homes in Chile (MINVU, 2018a) and the Energy Qualification Procedures Manual of Housing in

Table 2
Manually mapped main local climate zones (LCZ) in Temuco.

LCZ class	Satellite image	Low-level photograph/typical residential – temperature sensor image	Properties*
LCZ2 3			SVF = 0.46% H/W = 0.6–1.2 TRC = 6–7 BSF = 42% ISF = 47% AHF**= 35.51 W/m^2 **MBH**** = 9.4 **SCR***** = 0.69 **FSR*** = 0.98 UVC** = 3% UTC** = 2.15% SEL = C2–C3 LCU= Commercial/ Residential
LCZ6			SVF = 0.68 H/W = 0.3 TRC = 5 BSF = 27% ISF = 22% AHF** = 0.96 W/m^2 **MBH**** = 3.05 m **SCR**** = 0.28 **FSR**** = 0.44 UVC** = 24.6% UTC** = 6.2% SEL = ABC1–C2 LCU = Residential
LCZ6 3		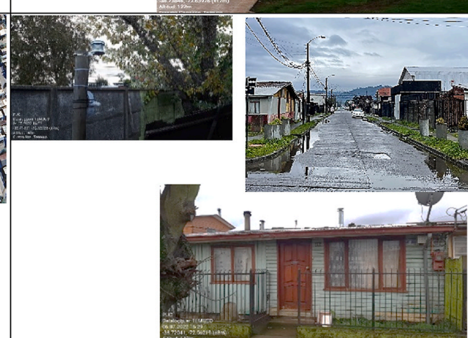	SVF = 0.62 H/W = 0.3–0.55 TRC = 6 BSF = 35% ISF = 38% AHF**= 14.18 W/m^2 **MBH**** = 3 **SCR**** = 0.52 **FSR**** = 0.39 UVC** = 14.8% UTC** = 3.3% SEL = D–E LCU = Residential
LCZ6 5	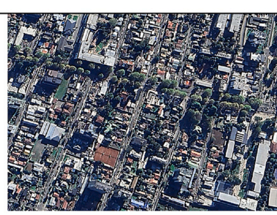		SVF = 0.54 H/W = 0.3–0.8 TRC = 5–6 BSF = 28% ISF = 33% AHF**= 28.07 W/m^2 **MBH**** = 7.6 **SCR**** = 0.29 **FSR**** = 0.62 UVC** = 22% UTC** = 9.9% SEL = ABC1–C2 LCU = Commercial/ Residential

Notes: SVF = sky view factor, H/W = canyon aspect ratio, TRC = terrain roughness class, BSF = building surface fraction, ISF = impervious surface fraction, AHF = anthropogenic heat flux, MBH = mean building height, SCR = site coverage ratio, FSR = façade-to-site ratio, UVC = urban vegetation coverage, UTC = urban tree coverage, SEL = socio-economic level, LCU = land cover use. (*) Values are averages of 1 km^2 of each urban area, except for AHF, which is vehicular traffic peak emissions. (**) Parameters used in the UWG simulation. Image references: Google Images.

Notes: SVF = sky view factor, H/W = canyon aspect ratio, TRC = terrain roughness class, BSF = building surface fraction, ISF = impervious surface fraction, AHF = anthropogenic heat flux, MBH = mean building height, SCR = site coverage ratio, FSR = façade-to-site ratio, UVC = urban vegetation coverage, UTC = urban tree coverage, SEL = socio-economic level, LCU = land cover use. (*) Values are averages of 1 km^2 of each urban area, except for AHF, which is vehicular traffic peak emissions. (**) Parameters used in the UWG simulation. Image references: Google Images.

Chile (MINVU, 2019).

CIBSE TM52 established a comprehensive approach to assessing the risk of overheating in free-running buildings, incorporating three criteria. If any zone or building fails two out of the three criteria, it is classified as overheated (CIBSE, 2013). The first criterion establishes a limit on the number of hours during occupied periods in the typical non-heating season, where the operative temperature exceeds the threshold comfort temperature by 1 K or more. The second criterion is related to the severity of overheating within a given day, acknowledging that both the temperature increase, and its duration contribute to the overall impact. Finally, the third criterion establishes an absolute maximum daily temperature for a room beyond which the degree of overheating is deemed unacceptable. According to CIBSE, the maximum value for ΔT shall not exceed 4 K from the operative temperature (CIBSE, 2013).

In ASHRAE Standard 55, the adaptive comfort model utilises the monthly mean outdoor air temperature, which is determined as the straightforward average of the preceding 30 daily average outdoor air temperatures (ASHRAE, 2010). Finally, the Dear and Brager Comfort Model (De Dear and Brager, 1997) proposes a regression equation that connects the neutral indoor temperature to the average monthly outdoor temperature (Enescu, 2017).

Notwithstanding, for the four building models, the hours not meeting the three adaptive comfort models during occupied hours were calculated. This was also done for the four LCZ classes in Temuco. To understand how UHI affects daytime and nighttime occupation zones, the unmet comfort hours were estimated separately for a living room and the main bedroom.

2.8. Sensitivity analysis

To comprehend the most important parameters that affect comfortability in naturally ventilated buildings influenced by UHI, a sensitivity analysis (SA) was conducted. An SA plays a crucial role in the initial design phase of buildings, aiding in the identification of key input parameters that can exert either a negligible or substantial impact on the output function (Maucec et al., 2021). In this research, the Morris SA method is proposed. The Morris screening method (Morris, 1991), rooted in the global sensitivity analysis technique, is particularly advantageous, as it focuses solely on identifying the most influential parameters. It stands out for its simple implementation and offers a computationally efficient alternative (Yang et al., 2016). The method can be described using Eq. (5):

$$EE_i = \left[y(x_i, \ldots, x_{i-1}, x_i + \Delta, x_{i+1}, \ldots, x_k) - y(\overline{x})\right]\big/_{\Delta} \tag{5}$$

where x_i, $i=1, \ldots k$ represents the input parameters and y represents the output results for the selected combination of parameters. The variable p represents the number of levels, and Δ is equivalent to [p/2(p − 1)] (Andrea et al., 2008). In the SA method, three indicators represent the importance of every design parameter, namely the mean (μ), the absolute mean (μ*) and the standard deviation (σ). Thus, the greater value that μ and μ* are, the greater the effect of the parameter in the output of the model. Similarly, the greater the value σ, the greater the interaction of a specific parameter with other parameters, which is a relevant indicator of nonlinearity. μ* can be used to classify the parameters in order of importance (Maucec et al., 2021), (Garcia Sanchez et al., 2014). These values are described in Eq. (6), Eq. (7) and Eq. (8):

$$\mu_i = \frac{1}{N}\sum_{r=1}^{n} EE_{i,r} \tag{6}$$

$$\sigma_1 = \sqrt{\frac{1}{N-1}\sum_{r=1}^{n}\left(EE_{i,r} - \mu_i\right)^2} \tag{7}$$

$$\mu_i^* = \frac{1}{N}\sum_{r=1}^{n}\left|EE_{i,r}\right| \tag{8}$$

where EE_{ir} corresponds to the *r-th EE* of X_i (Andrea et al., 2008). Additionally, according to Maučec et al. (2021), the relationship between the standard deviation and the absolute mean can be categorised into four effects: nearly linear (σ/μ* ≤ 0.1), monotonic (0.5 > σ/μ* > 0.1) or nearly monotonic (1 > σ/μ* > 0.5), as well as nonmonotonic or nonlinear effects, possibly involving interactions with other parameters (σ/μ* > 1). These effects can be visually discerned in a scatter plot by representing three straight lines with slopes of σ/μ* >0.1, 0.6 and 1. The SA simulation was performed using JEPlus + EA software Version 2.1 (Zhang and Jankovic, 2017). JEPlus + EA is an online platform optimisation engine that is coupled with JEPlus and EnergyPlus software for parametric and optimisation analysis. In this research, SA was conducted in two optimised houses in both socio-economic districts (L_PDA and M_PDA), meaning houses with the restrictive PDA standard. These models were run during the four hottest months (December to March). Building parameters and corresponding ranges that were sensitised are described in Appendix B.

3. Results

3.1. Urban classification

In this research, two urban classification types are relevant: morphology and socio-economic grouping. Fig. 3 illustrates the LCZ classification and socio-economic level (SEL) of Temuco. Fig. 3b demonstrates the LCZ map derived from satellite images and WUDAPT algorithms, following the methodology outlined by the WUDAPT portal. Through multiple iterations, an overall accuracy of 0.70 was achieved. The figure highlights that LCZ6 and LCZ3 are the primary classes identified by the algorithms, with smaller portions of LCZ2 and LCZ5. To accurately capture Temuco's urban characteristics, a manual LCZ map was created using a tailored methodology, due to the city's diverse urban landscape. Consequently, an LCZ subclass was defined, combining features from two classes to better represent actual urban conditions (Stewart and Oke, 2012). Fig. 3a reveals the manually configured LCZ map, emphasising four predominant types: $LCZ2_3$, LCZ6, $LCZ6_3$ and $LCZ6_5$. These represent 4.5%, 18.7%, 39.8% and 6.8%, respectively, which is 70% of the city. $LCZ2_3$ represents the city centre, with predominantly commercial use but some residential as well. $LCZ6_5$ constitutes mixed predominant uses, while LCZ6 and $LCZ6_3$ stand for residential zones. These four LCZ classes were employed for subsequent analyses. Table 2 provides an overview of the main LCZ classes in Temuco, along with their calculated properties within a 1 km^2 area (1000 × 1000 m) for each urban region. Fig. 3c outlines the socio-economic levels associated with each LCZ, as officially defined in the country's latest census (INEa). Here, the higher socio-economic classes (ABC1 and C2) represent 40.95%, while the lower classes represent 59.05%. One interesting observation in Figs. 2 and 3 is that $LCZ6_3$ and lower socio-economic classes tend to coincide.

3.2. UHI intensities

Table 2 depicts the urban parameter results, which are relevant to the UWG simulations. MBH, SCR and FRS strongly contribute to the UHII (Salvati et al., 2019), (Nakano et al., 2015). Considering these values, alongside AHF, UVC, UTC and LCU surfaces customised in every predominant LCZ class, the annual simulation in UWG generated the UHII in Fig. 4. Conversely, Fig. 5 shows UHII measured during the six-month period in the year 2022. Comparing these results with the parameters in Table 2, there was a clear positive correlation between denser urban areas and UHII, as expected. However, when comparing Figs. 4 and 5, some variations are highlighted. In the modelled UHII, the

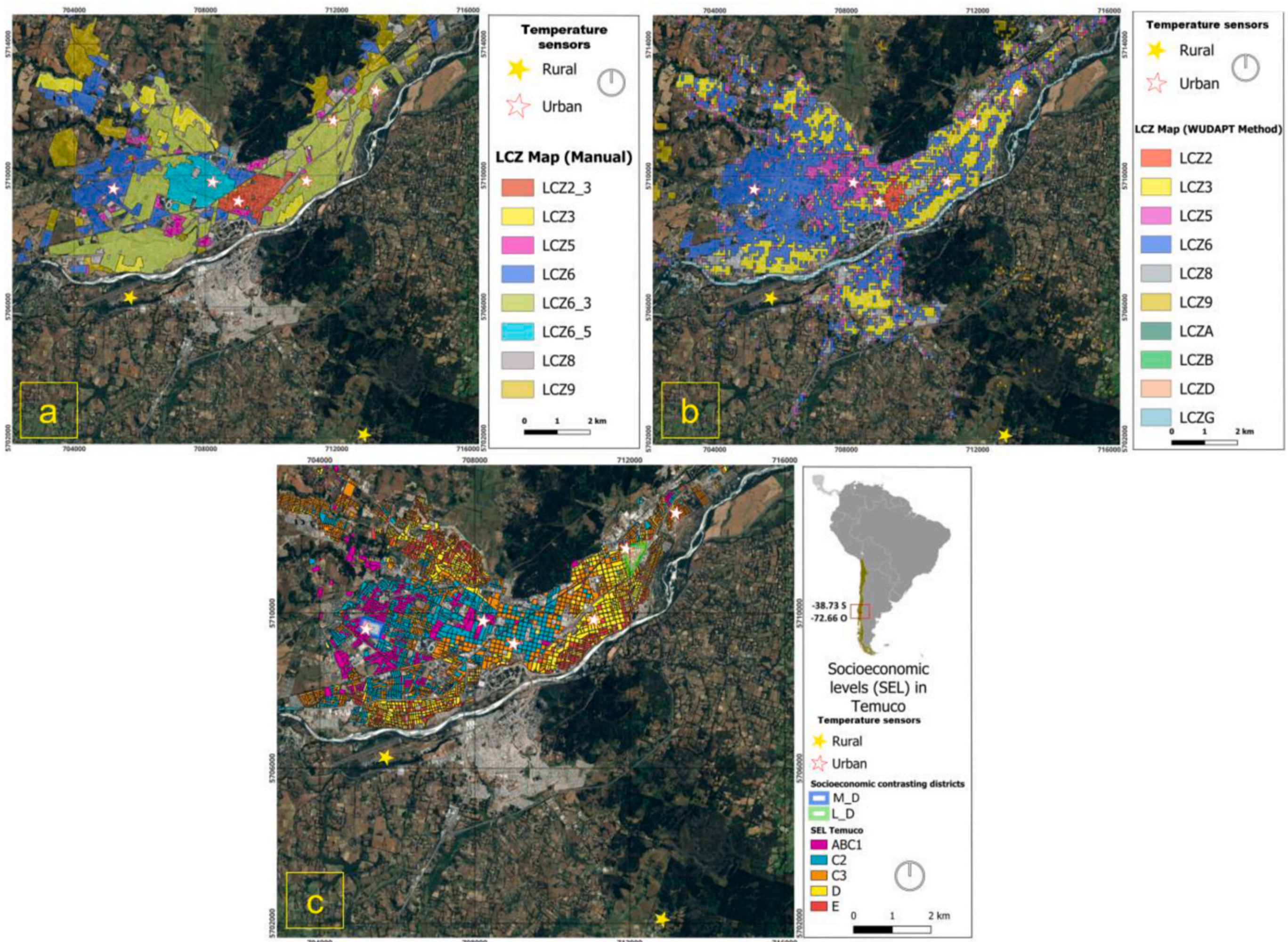

Fig. 3. Main local climate zones (LCZ) mapped (a) manually (b) and using the WUDAPT methodology, with (c) socio-economic levels in Temuco.

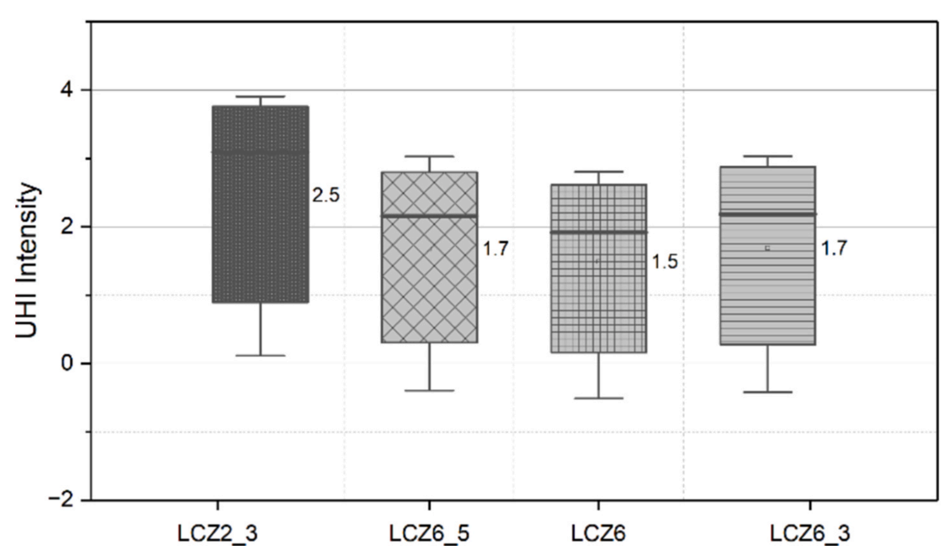

Fig. 4. UHII results modelled in UWG.

values range between 1.5 and 2.5 °C for LCZ6 and $LCZ2_3$, respectively, while in the UHII field measured, this reached 1.6 °C for $LCZ2_3$ and 1.3 °C for LCZ6 and $LCZ6_5$. These disparities are due to several factors. First, UHII modelling was performed based on EnergyPlus Weather Format files (.EPW files), which contain weather data from several years, to perform a typical and representative year-to-energy simulation. Thus, it is not accurate to compare UWG results with short-term field measurements. Location sensors can also influence the measurements

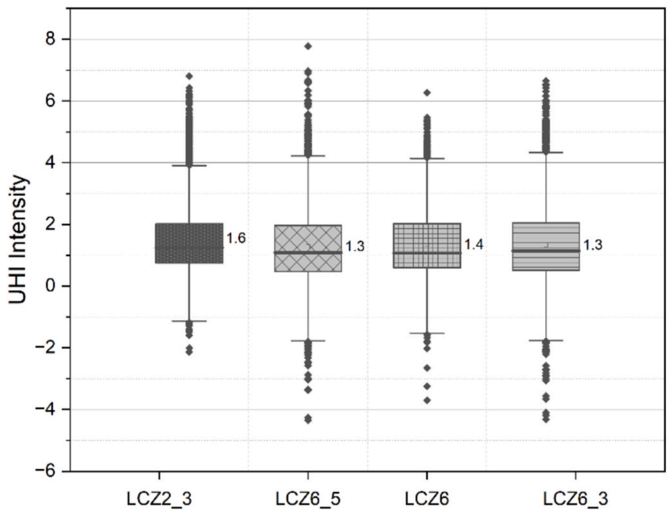

Fig. 5. Filed measurement results for UHII (December 2021 to June 2022).

and results. For example, although in this research optimal sensor locations were procured, it is possible that the sensors located in $LCZ2_3$ did not represent the actual conditions of downtown Temuco (see Table 2) because it was unviable to site them in the most accurate place due to the risk of theft, and another local restrictions.

Additionally, two rural measurements were compared, as illustrated in Fig. 2. Specifically, we compared data from the Maquehue Meteorological Station (Meteochile) with information collected from an installed rural datalogger, employing metrics such as root mean square error (RMSE) and mean absolute percentage error (MAPE). The temperature readings from the rural HOBO datalogger also spanned December 2021 to June 2022, a six-month period. This dataset was then juxtaposed with the corresponding timeframe obtained from the Maquehue station. The analysis revealed an RMSE of 1.6 and a MAPE of 7.8%, both falling within an acceptable range compared to findings in similar literature (Bueno et al., 2013), (Litardo et al., 2020). The observed error can be attributed to variations in both instruments and locations.

3.3. Indoor temperature measurements

Considering that the focus of this research was to evaluate socio-economic differences in the thermo-energy performance of housing districts, sample houses were monitored during six months in L_D and M_D. Fig. 6 reveals indoor temperature measurements during the first week of summer in 2021. Both measurements show the living rooms of L_PDA and M_PDA houses naturally ventilated and with similar orientations, which are in $LCZ6_3$ and LCZ6, respectively. Here, it is possible to detect how L_PDA can suffer disparities between indoor and outdoor temperatures that are eventually higher than 8 °C, unlike M_PDA, where maximum differences are near 5 °C. These distinctions relate to the specific building conditions of both houses, such as the size of indoor spaces, window openings etc., but are also affected by users' behaviour (e.g. ventilation zone decisions). Although these differences are independent of the UHI effect, the consequences of thermal comfort or eventually cooling energy loads worsen, considering the urban microclimate. Notably, the Netatmo sensor also registered daily UHII differences higher than 4 °C between the L_D and M_D, as predicted by UWG simulations (Fig. 4).

3.4. Building model verification

As presented in the methodology section, the verification process is divided into three-step analyses: parameter settings relevant to ground temperature model calculation, heating load adjustment and verification, and indoor temperature comparison.

3.4.1. Ground temperatures

Thermal conductivity, density, and the moisture content of soil within L_D and M_D were field measured and then calculated to set as input parameters in EnergyPlus. Regarding the approaches that the software allows to characterise ground heat transfers, models L_OGUG, L_PDA and M_PDA were simulated with three methods, namely: (i) the default ground temperatures in EnergyPlus (18 °C for the whole year), (ii) the slab pre-processor model with customised inputs (Vanessa Aparecida and Karin Maria, 2017) and (iii) the finite difference model with default and customised inputs. For more information about these or other ground temperature models, the reader is referred to the EnergyPlus documentation manual (Bigladder Software).

Table 3 discloses the values obtained for field measurement and

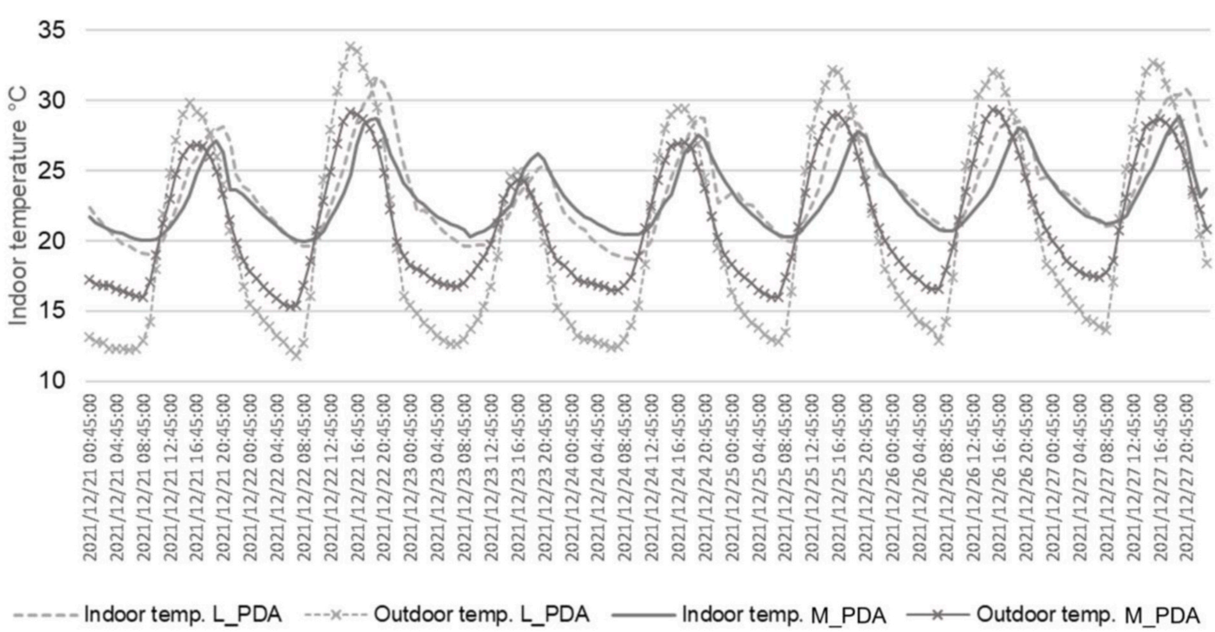

Fig. 6. One-week indoor temperature measurements in sample houses in $LC6_3$ (L_PDA) and LCZ6 (M_PDA).

Table 3
Input parameters used for ground temperature models in EnergyPlus.

	L_OGUC and L_PDA		M_PDA	
	Default values used (*)	Measured values	Default values used (*)	Measured values
Soil thermal conductivity (W/mK)	1	0.66	1	0.72
Soil density (kg/m^3)	1200	1302.89	1200	1465.71
Moisture content (%)	30	36	30	30

(*) Parameter extracted from the Slab-preprocessor manual (Vanessa Aparecida and Karin Maria, 2017).

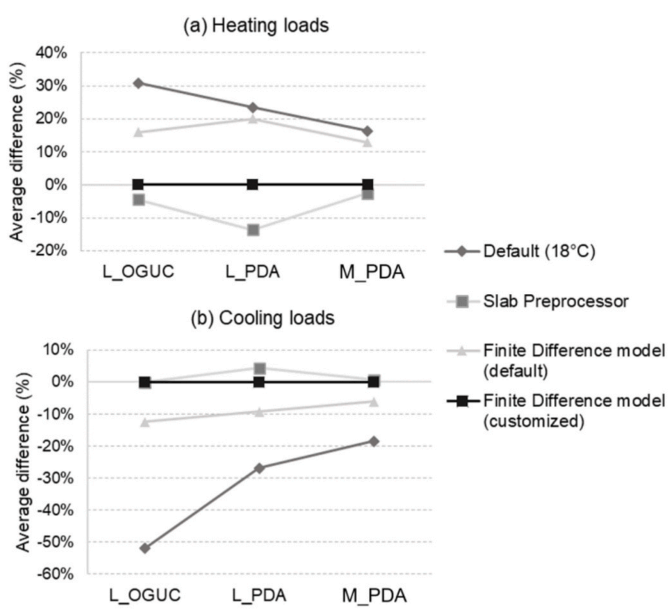

Fig. 7. Comparison results between ground temperature models within EnergyPlus: (a) annual heating load performance difference and (b) annual cooling load performance difference.

calculations, and Fig. 7 shows the percentage differences in (a) energy heating loads (b) and energy cooling loads in an annual simulation. Significantly, differences between models range between −13.6% and 30.8% in heating loads and between 4.41% and −51.9% in cooling loads. Even when Table 3 does not show larger differences, the relevant alterations are displayed in Fig. 7. Clearly, the default ground temperature of 18 °C was far from the detailed ground models, highlighting the importance of accurate approaches when these types of buildings are evaluated through a simulation process. This is also remarkable when the finite difference model performs up to 20% differently in L_PDA heating loads compared with the same model, but with adjusted inputs. Conversely, the slab-preprocessor performed similarly to the finite difference model because both used measured input parameters from Table 3. Importantly, the differences also depend on the overall input parameter in every model. For example, in less isolated models, such as L_OGUC, these variations are bigger than in the same model but with more restrictive whole-building parameters (L_PDA).

3.4.2. Heating load comparison

For better comparison, the cardinal position was set equal to real buildings, and infiltration rates were also adjusted in simulation models. Furthermore, for every verification process, it was necessary to set stove efficiencies according to every model. Consequently, according to previous local research, for the L_OGUC model, the firewood stove efficiency was set at 0.41 (Larrea-Sáez et al., 2023), (Camarasa et al., 2022). For L_PDA and M_PDA, it was set at 0.6 (Camarasa et al., 2022), while the pellet efficiency was set at 0.85 (Camarasa et al., 2022). Table 4 shows the percentual difference between these results and the simulation results in EnergyPlus after the infiltration rate adjustments. Moreover, considering that indoor air temperature measurements were kept during the initial heating season months (April to June), it was possible to measure indoor temperatures during this time, which means users spontaneously procured an approximate setpoint. Average temperatures ranged are also showed in Table 4. Notably, the L_OGUC and L_PDA models performed very similarly to real houses (lower percentual difference) when the setpoint was 20 °C, while M_PDA performed the best fit with the setpoint at 21 °C. Significantly, higher socio-economic levels (M_PDA) could be investing more energy in hotter or better thermal indoor conditions.

3.4.3. Indoor temperature comparison

Indoor temperatures in hourly frequencies were measured in sample houses in L_D and M_D during summer and autumn (year 2022) for the verification process. Fig. 8 demonstrates the results of air temperature measurements in two indoor spaces compared to the same thermal zones simulated after the synchronised adjustment of infiltration rates for heating consumption verification. In L_D, measurements and comparisons were made in two building conditions: L_OGUC and L_PDA. While L_OGUC are houses with at least the mandatory energy standards demanded in the country, L_PDA and M_PDA are houses with newer and more restrictive standards demanded in the city. House models were set with the parameters stated in Appendix A; the unique exception was the infiltration rates, which were first set with parameters from regional standards (Appendix A), but afterward were adjusted according to the proposed verification process. Fig. 8 denotes that measurements in sample houses had slightly lower average temperatures in January and February compared with modelled temperatures, with March as the only month with the opposite trend. This adjustment was made to ensure that the simulation yielded conservative results, thus avoiding overestimation results.

Table 5 describes the values of CV (RMSE) and NMBE for every thermal zone and model evaluated. According to ASHRAE Guideline 14, to validate simulations for an entire building, the NMBE should be less than 10%, and the CV(RMSE) should be below 30% when comparing hourly data, which means that the lower these values, the better calibrated the models (Zuhaib et al., 2019). Previous research has used these indexes to compare indoor temperature measurements and obtained similar CV (RMSE) results to those obtained in this research (Aparicio-Fernández et al., 2019), (Ogando et al., 2017), which are within the proposed criteria. In contrast, the results failed the NMBE index criteria. However, the results were considered acceptable for the next evaluation processes in the present research, considering that positive NMBE values indicate the simulation is forecasting below the

Table 4
CV (RMSE) and NMBE results for the indoor air temperature of simulation models in each thermal zone.

Index	Living L_OGUC	Bedroom L_OGUC	Living L_PDA	Bedroom L_PDA	Living M_PDA	Bedroom M_PDA
CV (RMSE) (%)	3.18	0.27	7.96	0.38	2.03	1.27
NMBE (%)	14.49	13.96	10.98	9.8	10.88	10.84

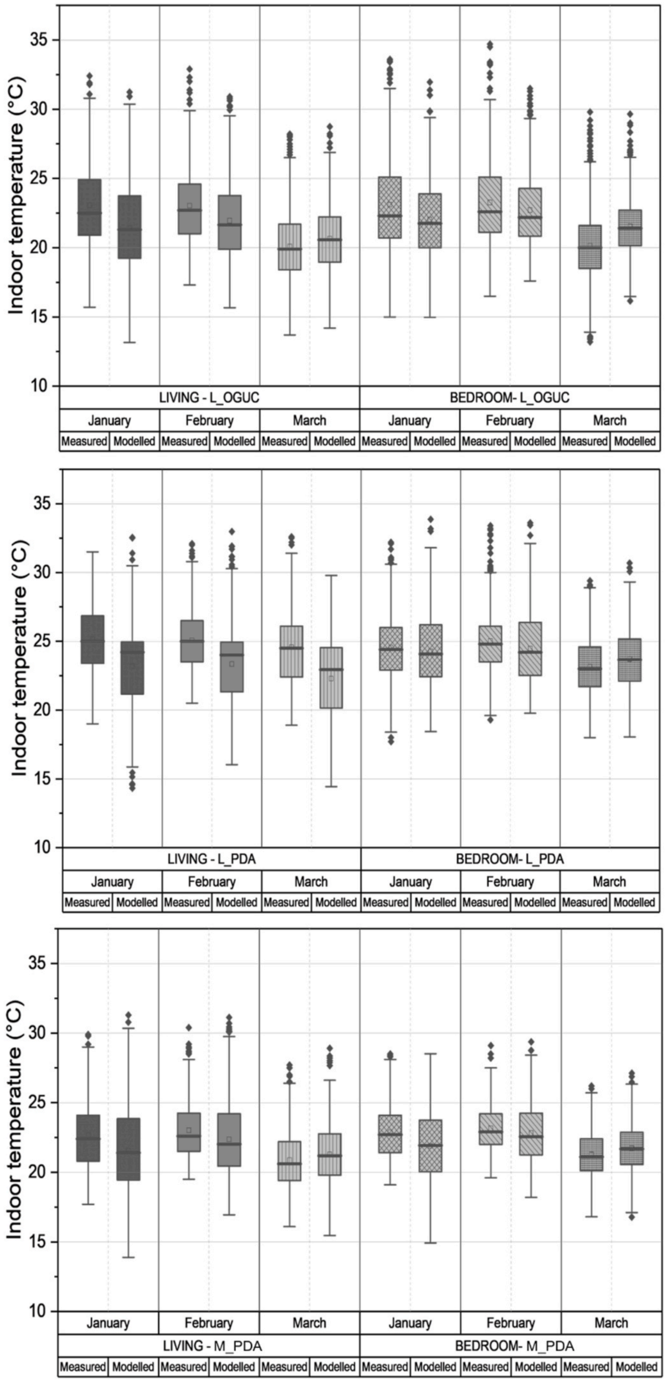

Fig. 8. Indoor temperature measurements vs. indoor temperature modelled for three summer month periods in the living rooms and bedrooms of three house models.

Table 5
Percentual differences between simulated and calculated annual heating loads.

	L_OGUC		L_PDA		M_PDA	
Simulated setpoint (°C)	19	20	19	20	20	21
Performance difference (%)	−16.44	1.98	−17.83	0.66	−13.42	3.59

measured data (Aparicio-Fernández et al., 2019).

3.5. Energy loads

Considering the UHI effect on building energy performance, in this research, four models (Table 1) were finally simulated in their corresponding socio-economic urban areas (e.g. L_OGUC in $LCZ6_3$). Nonetheless, every model was also simulated in the four LCZ classes that characterised Temuco city (Table 2). This approach was selected to understand how one specific residential model could perform differently, depending on the urban zone where it is located. These produced 16 urban model simulations plus four reference models, which were performed with rural climate files as a reference for comparison. Fig. 9 depicts the results of annual cooling and heating loads (over the net-conditioned building area). Fig. 10 demonstrates the percentual variations between energy loads and rural references.

As expected, the UHI effect influenced energy-building performance (Fig. 10). Unsurprisingly, the denser the urban zone, the more UHI impacted performance. Considering the methodology presented by (Lopez-Guerrero et al., 2023), the cooling penalty due to the increase of one degree of temperature or UHII by surface building resulted in between 3 and 3.5 kWh/m^2/year/K (depending on the LCZ class), which is lower than the world average presented by the authors for residential use. Because of the predominant colder climate in Temuco city, cooling loads are still low in absolute terms, ranging between 21 and 25 kWh/m^2/year for semi-detached houses. However, these values are up to five times higher than the limits proposed in the sustainability national standard for the climate zone, which are 5 kWh/m^2/year for 2020 and 0 kWh/m^2/year until year 2040 (MINVU, 2018a). Moreover, when a typical flat is set with newer regional thermal requirements (PDA), this difference is quite higher. In this sense, it is remarkable that M_FLAT is overloaded regarding cooling requirements. This could be explained by the large quantity of windows allowed and the window type recommended for updated standards (see Appendix A), alongside reduced wall area to dissipate received energy (just two walls and no floor or roof has outdoor boundary conditions). If the UHI effect is considered, this issue is obviously worse.

Conversely, the UHI effect helps to diminish heating loads in proportions ranging between −20.47% and −81.95%, depending on the model and urban zone (Fig. 10). Indeed, these effects ensure that the limits proposed in the sustainability national standard for heating loads never exceed those proposed for 2020 (135 kWh/m^2/year) (MINVU, 2018a). Fig. 9a also illustrates that the newer energy requirements help to diminish heating loads; however, there is quite a slow influence on cooling loads. This is explained because the PDA standard focuses on the heating season as the predominant climate, though UHI or global warming effects are poorly considered. Additionally, when the same model is hypothetically located in different urban zones, some distinctions in energy loads can be observed, the main ones being around 16%–24% in semi-detached models for heating loads and between 10% and 16% for cooling ones. These results highlight the importance of pondering urban parameters when energy performance is measured even in the same city.

3.6. Thermal comfort

Similar to Section 3.5, all models were simulated in their corresponding urban zone but were also hypothetically located in four main LCZ classes in Temuco city. Fig. 11 displays the results of discomfort hours in every model and all buildings and urban zones. These results are divided into two indoor thermal zones: a living room for daytime use and a bedroom for nighttime use. In addition, they were simulated during summer seasons as a naturally ventilated regime.

As observed in Fig. 11a and c, the Dear and Brager and ASHRAE 55 (2010) models performed relatively similarly in the number of hours, whereas CIBSE TM52 performed with less discomfort time. However,

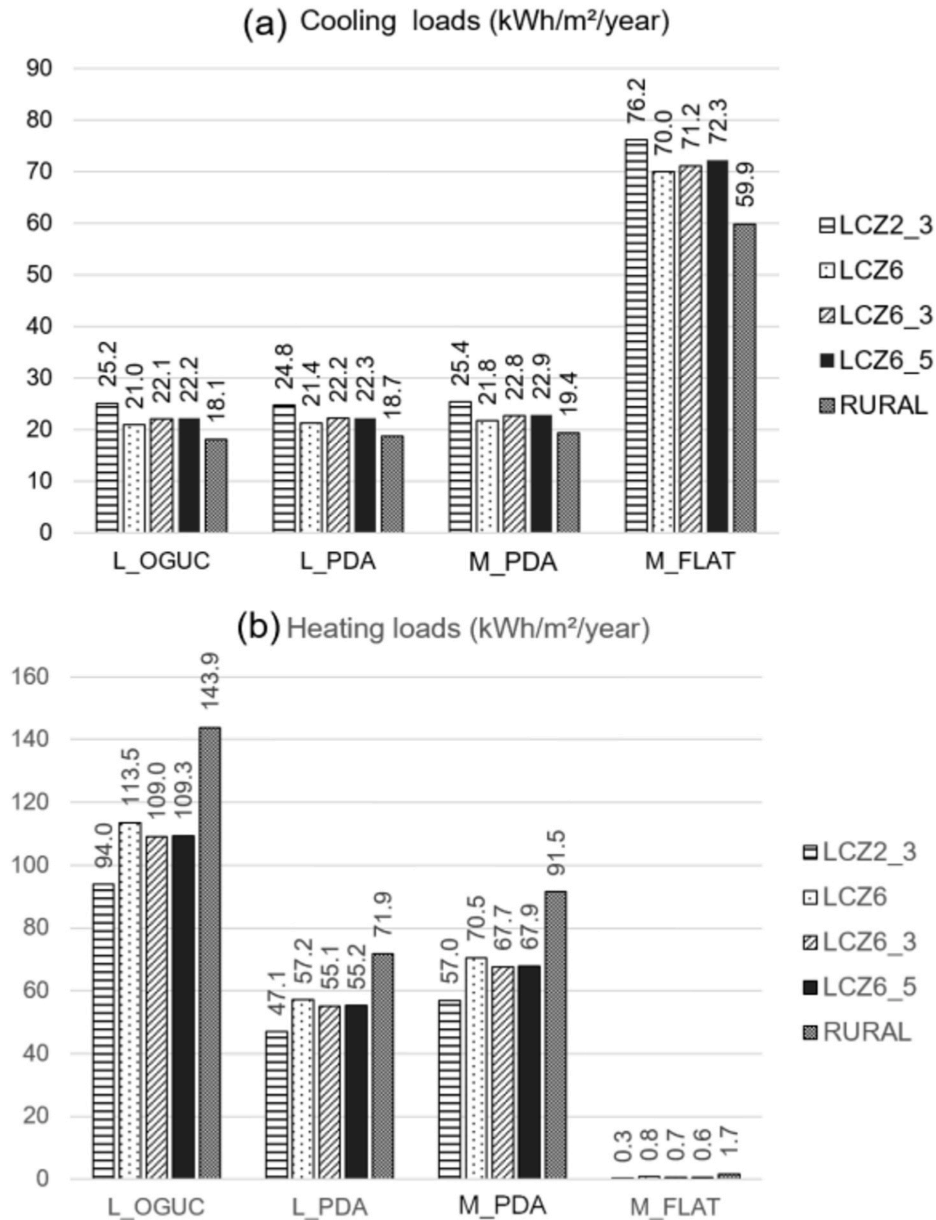

Fig. 9. Normalized annual (a) cooling and (b) heating loads of four urban models and rural references.

according to the CIBSE TM52 model and the overheating criteria proposed, all living rooms in all urban zones exceeded 3% of hours in discomfort conditions in occupied hours, therefore failing the first criterion. The percentual range of discomfort hours in the living room ranged between 11.5% and 23.7% in semi-detached house models, while in M_FLAT ranged up to 67.2% depending on the LCZ class. In the case of bedrooms, the discomfort time was always under 3% in semi-detached houses but exceeded in M_FLAT between 15.9% and 24.4%. Regarding the severity of overheating within a given day (second criterion), the results were similar to the first criterion, where the living room always exceeded several weighted exceedance days, having 14 and 34 in semi-detached house models, whereas n M_FLAT ranged up to 81 depending on the urban zone. This criterion was also not complied in the bedroom for M_FLAT. However, no weighted exceedance days resulted in semi-detached houses. Finally, the last criterion of absolute maximum daily temperature behaved similarly. Here, the living room always exceeded several days above this temperature, ranging between nine and 34 in semi-detached house models, while in M_FLAT, it ranged up to 35 depending on the urban zone. Likewise, only M_FLAT surpassed the limit by up to 41 days. Thus, it is possible to affirm that according to the CIBSE TM52 model and the overheating criteria proposed, daytime spaces present overheating in Temuco city for the residential model analysed. Nonetheless, nighttime spaces present overheating only in typical residential departments (M_FLAT) upgraded with new energy local standards. Meanwhile, the comfort models presented in Figs. 11a and c revealed a major number of discomfort hours, highlighting that the risk of overheating is also alerted in these models.

If residential semi-detached houses are analysed in their respective urban zones in Temuco, it means L_PDA (or L_OGUC) in $LCZ6_3$ and M_PDA in LCZ6. Notably, the impact of UHI on comfort hours depends on the socio-economic status of the model's location. Results demonstrate that the impacts on the living room are 56.2%, 76.5% and 50.2% higher in L_D, considering Dear and Brager, CIBSE TM52 and ASRHAE 55 (2010) comfort models, respectively (Fig. 11a, b and 11c). Moreover, the ASRHAE 55 (2010) comfort model demonstrates the bedroom performed 100% worse in the low-income model. In absolute terms, this difference was only 12 h (Fig. 11c). Fig. 11 also conveys that L_OGUC performed with 82.3%, 65.5% and 57.9% fewer discomfort hours than

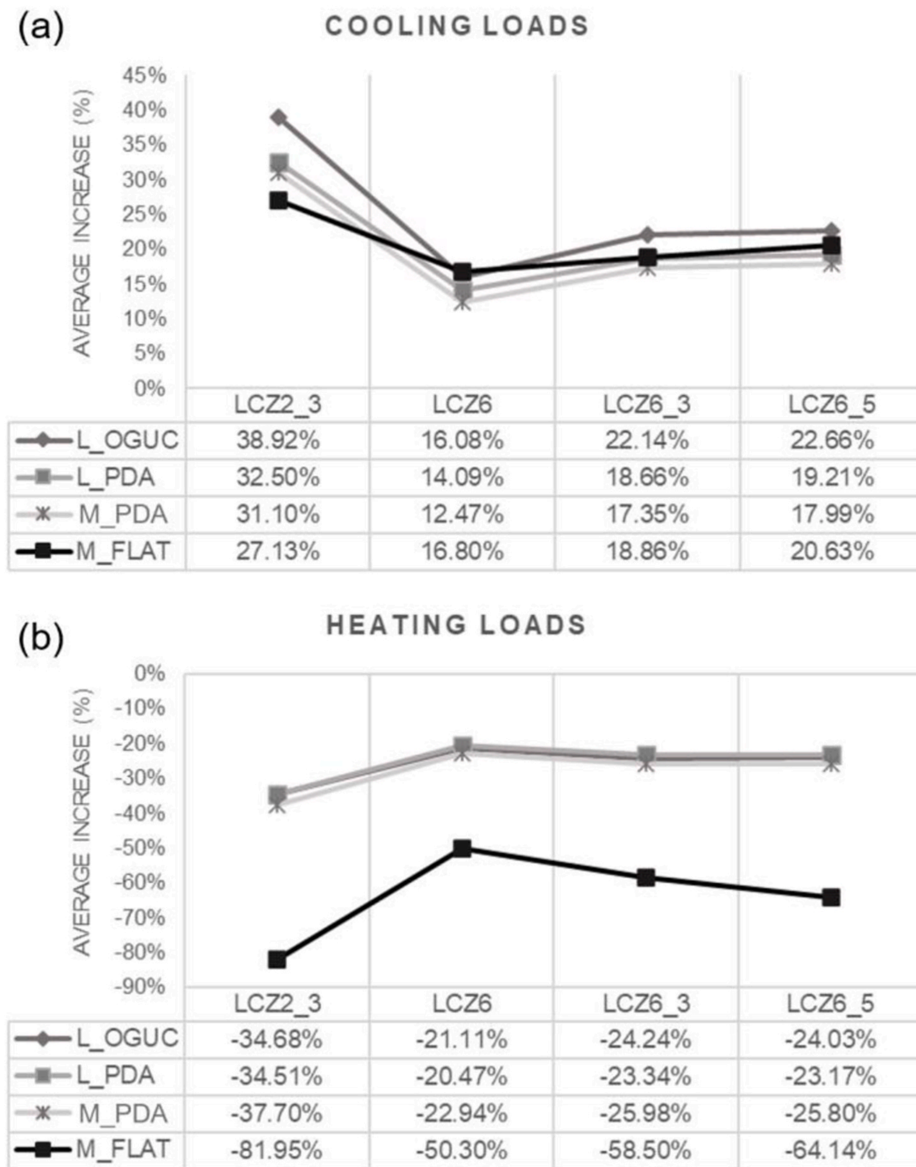

Fig. 10. Percentual differences between (a) cooling loads and (b) heating loads compared to rural references in the same urban zone.

L_PDA for the Dear and Brager, CIBSE TM52 and ASRHAE 55 (2010) comfort models, respectively. These outcomes highlight how UHI could impact thermal comfort differently depending on locations within the same city and socio-economic factors.

Regarding the impacts caused by UHI in comfort time, Fig. 12 shows the percentual difference in hours regarding rural climate. The negative impacts range from 0.5% to 100% depending on the residential model, LCZ class, thermal zone and, obviously, comfort model. As expected, the denser the urban area, the higher the UHI impact in discomfort time, being $LCZ2_3$ and $LCZ6_5$ the urban zones with likely major percentual differences. For daytime use spaces, percentages in varying LCZ classes average 23.1%, 5.5% and 6% for the Dear and Brager, CIBSE TM52 and ASRHAE 55 (2010) comfort models, respectively. Similarly, for night-time use spaces in the M_FLAT model, this average is 15.6%, 47.8% and 52.8%, respectively. Significantly, the percentages in Fig. 12 are calculated in every model in relation to the rural climate for any LCZ class and comfort model results. Hence, they are not comparable. In contrast, an interesting result that draws attention is the greater discomfort hours present in rural models in the living of L_PDA and M_FLAT (Fig. 12). Further analysis of these counterintuitive results indicated that during some daytime-occupied hours in Temuco, an urban cool island effect (UCI) was presented in certain urban zones (Figs. 4 and 5). As an example, Fig. 13 shows the UCI intensity in the $LCZ2_3$ class. Here, 9.4% of afternoon occupied hours in the summer season are lower than rural temperatures. UCI has been encountered in other studies (Duan et al., 2018), (Yang et al., 2017) and can be produced during daytime hours, among other factors, for the thermal mass of building and roads (Yang et al., 2017).

It also is important to highlight that UGW simulation results do not alter solar radiation in EPW files. Accordingly, buildings with a higher proportion of windows, which is the case of the L_PDA, M_PDA and M_FLAT models, are more sensitive to solar incidence.

Significantly, bedroom spaces performed without any discomfort hours in semi-detached houses are related to the predominant weather conditions of Temuco, where the daily thermal amplitude is higher and can reach up to 25 °C on some summer days. Thus, even with the UHI effect, nighttime temperatures in the heating season used to be low enough to keep comfortable conditions in adaptive comfort models, where users' behaviours can theoretically control such circumstances.

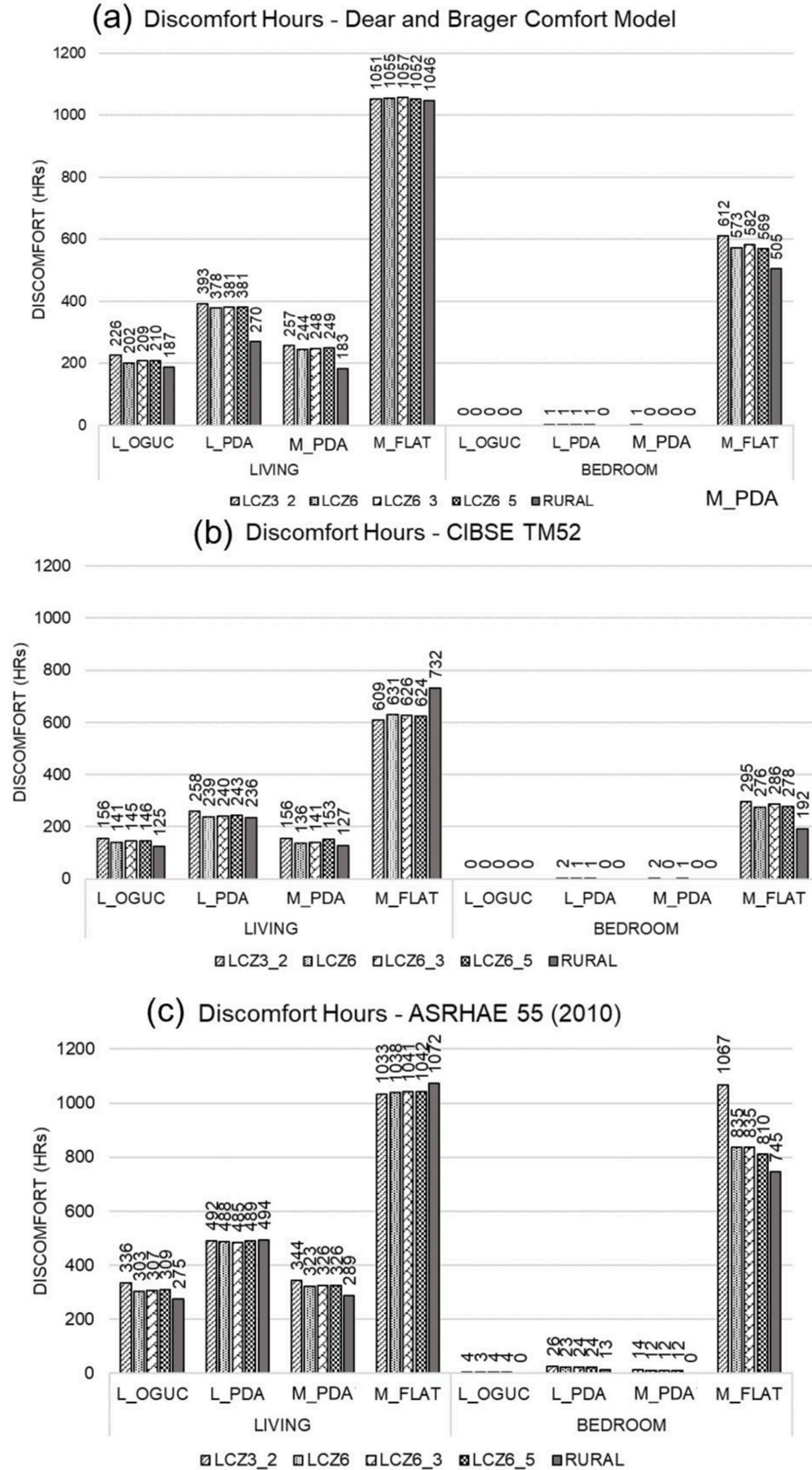

Fig. 11. Discomfort hours in all models and urban zones according to (a) the Dear and Brager comfort model, (b) the CIBSE TM52 comfort model and (c) the ASHRAE 22 (2010) comfort model.

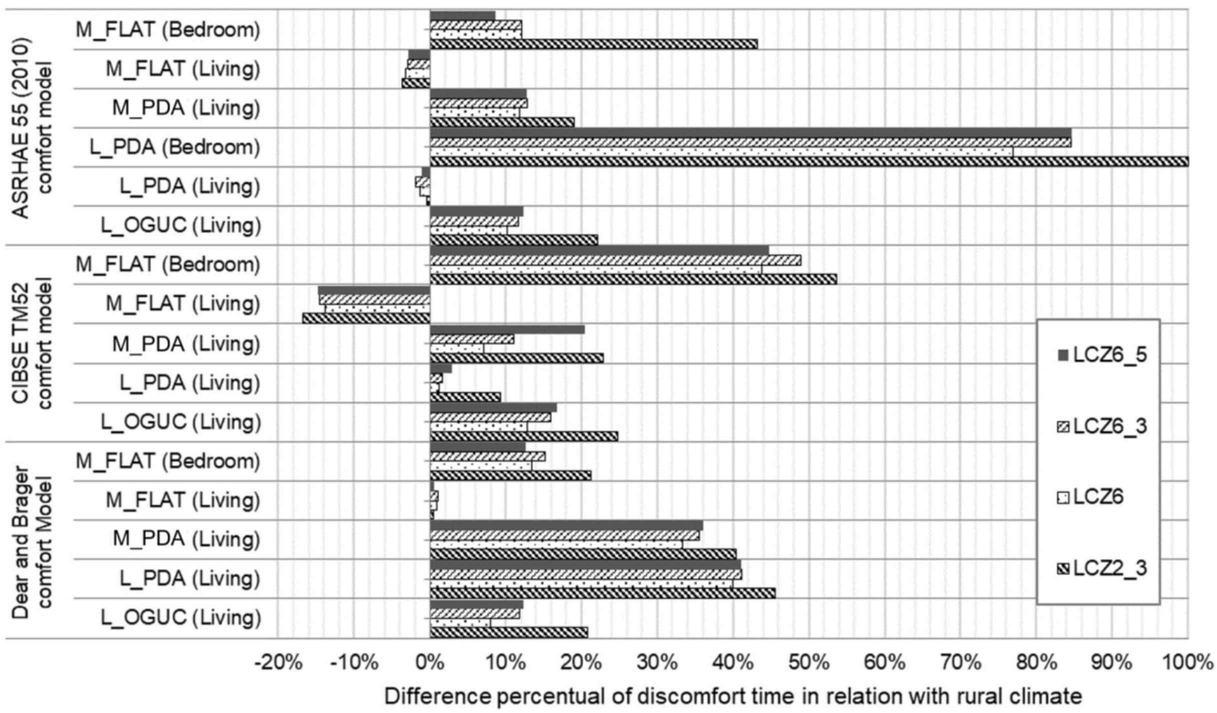

Fig. 12. UHI impacts comfort time in thermal zones according to the three adaptive comfort models. Observation: Some bedroom results were not shown because of the absence of discomfort time.

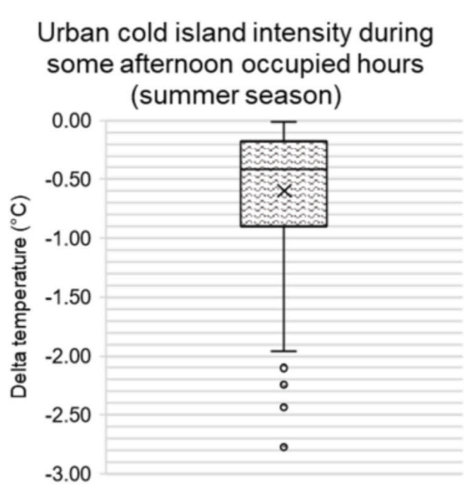

Fig. 13. Urban cold island during afternoon hours in the summer season.

3.7. Sensitivity analysis

Finally, to gain a deeper understanding of the key parameters influencing the thermo-energy performance of the analysed buildings, a sensitivity analysis (SA) was conducted during the summer. The focus was two main outputs: cooling loads (kWh) and discomfort time (hours), according to the adaptive model ASHRAE Standard 55, maintaining a 90% acceptability limit (refer to Section 2.7.2). Additionally, within the scope of this research, which centres on socio-economically diverse districts, SA was exclusively conducted on semi-detached models adhering to the PDA standard (L_PDA and M_PDA). This choice assumes that this normative pursues to optimize the OGUC standard. Appendix B presents the parameters' analized. Figs. 14 and 15 display the SA results.

Fig. 14a reveals that the most influential parameters for cooling loads in the L_PDA model are the window-to-wall ratio (WWR) and building orientation, followed by solar transmittance and solar absorptance. The effect of these parameters is almost monotonic to monotonic, indicating a strong interaction between them and a constant linear relationship between the parameter and cooling loads. These same trends occur in Fig. 14b with the discomfort time in L_PDA, where solar absorptance, wall heat capacity, solar transmittance, orientation, wall insulation and ventilation rate ranked as the most influential parameters. In the case of Fig. 15a and b, the results are similar in a ranking of influence for cooling loads and discomfort hours for M_PDA, with almost all parameters within the monotonic region. The exceptions are wall insulation for cooling loads in both models, orientation for discomfort hours in L_PDA and orientation for cooling loads in M_PDA, which are in $\sigma/\mu^* > 1$ with non-linear effects. Nevertheless, for the case of the orientation of L_PDA, they still affect the high variability of the outcomes.

Although the most influential parameters in both models were similar, there were remarkable differences. In cooling loads, solar absorptance and orientation became less important in M_PDA compared to L_PDA, highlighting that, probably in L_D, urban arrangement and albedo properties could benefit residences' energy performance, while in medium-high-income districts, glazing properties could be more important. This reasoning is even more remarkable in Fig. 15a and b, where solar transmittance and solar absorptance became important parameters for comfort time perception. Similar to the cooling performance results, the albedo properties of walls and roofs are quite important strategies in L_D. Likewise, solar absorptance is not negligible in M_D but has less influence than solar transmittance. This result is interesting considering that changing the colour properties of exterior surfaces is the simplest or cheaper strategy for application in L_D. Another parameter that features in L_PDA models is wall heat capacity. This is quite important in southern cities in Chile, where wooden or light building materials are more popular, especially in L_D, and heavy materials (concrete or bricks) are more common in higher-income neighbourhoods. Wall insulation also has an important influence on comfort conditions in both models, which is equally important in heating seasons. Finally, in the L_PDA model, ventilation rate, which could also be a simple strategy, has a relevant impact on comfort conditions, whereas

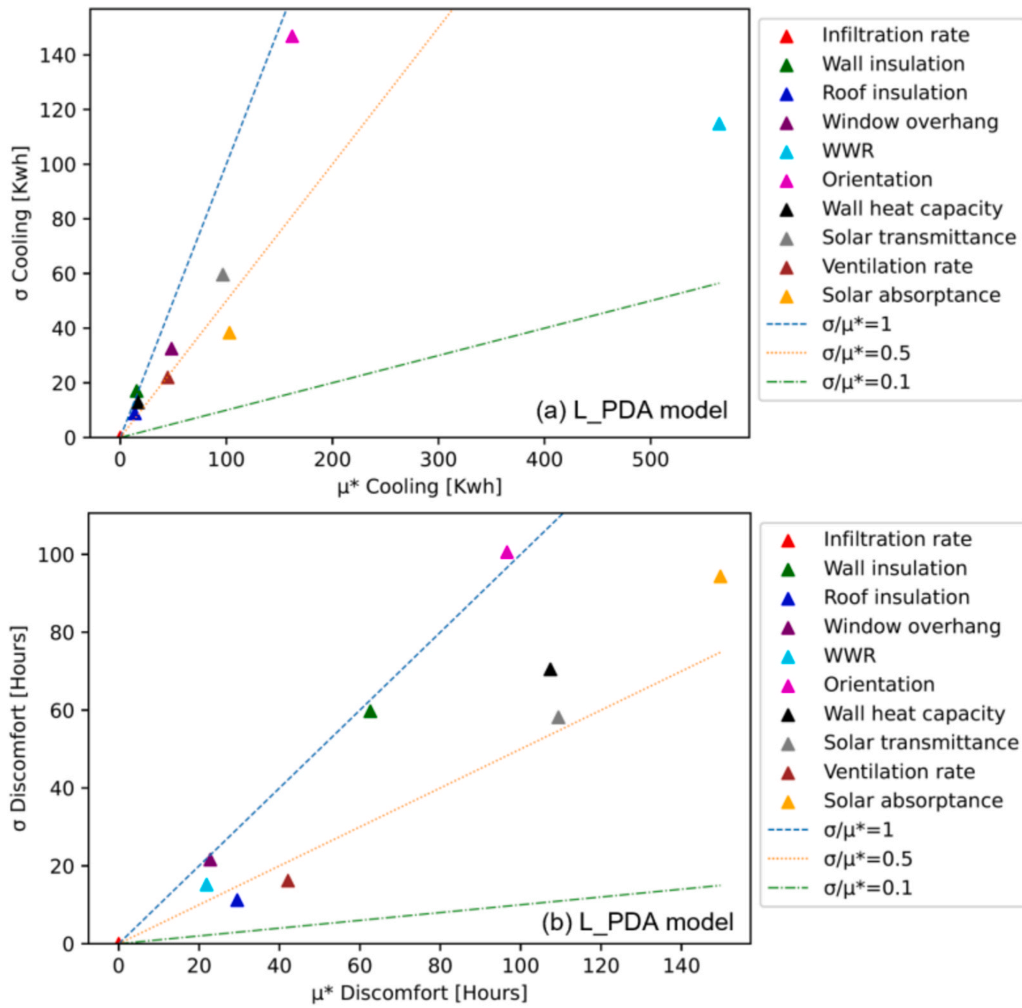

Fig. 14. Sensitivity analysis results in (a) L_PDA cooling loads and (b) L_PDA discomfort hours.

M_PDA overhang installation could be influential in a similar way.

4. Discussion

4.1. UHII and socio-economic issues

This research examined the scale of a small-to medium-sized city with a historically predominant colder climate. Surprisingly, the UHI effect was observed with a comparable intensity to that found in larger cities, as presented by (López-Guerrero et al., 2022). Moreover, urban buildings could be affected unequally according to their socio-economic statuses and the urban tissue to which they belong. This research demonstrated this trend in Temuco city. Although there were no remarkable UHII differences between low and medium–high districts, it means that regarding absolute differences, these disparities can be noted in relative terms when evaluating houses belonging to each neighbourhood. Furthermore, when the same building model is hypothetically placed in different urban zones, distinctions can reach up to 16.6% and −20.7% for cooling and heating loads, respectively, in the case of the L_OGUC model (Fig. 9). Hence, building design and urban tissue have quite close dealings that are commonly underestimated, especially in buildings' energy-efficiency codes. Therefore, it is important to build an urban-building well-balanced design to equally dole out the fair benefits of thermal comfort and energy outlays.

Achieving more equitable thermal urban conditions is still an intricate challenge, considering the complexity of urban behaviour. As observed in Table 2, L_D exhibit disadvantageous urban indices compared with high–medium-income ones. Thus, any implementation of energy standards starts from a point of shortcoming. This issue is commonly encountered in many cities in either developed or developing countries (Lin et al., 2023), (Kronenberg et al., 2023), (da Silva et al., 2023b), (de Castro Mazarro et al., 2022) and has been identified as among the main triggers of urban overheating (Eugenio Pappalardo et al., 2023), (Sarricolea et al., 2022). According to regional indicators (INEb), Temuco presents a green area which is near to the international recommendation of the World Health Organization of 9 m^2/person (WHO, 2009). In addition, Temuco complies with the indicator of public squares per inhabitant 400 m away (INEb). However, these areas are not distributed equally. The reasons for this are diverse but could relate to green gentrification (García-Lamarca et al., 2022), (Bockarjova et al., 2020), which is the effect of increased urban land prices due to renovation in certain areas, displacing poorer residents to inadequate urban zones (Bockarjova et al., 2020). In addition, the effects of land speculation prices contribute to these disparities, causing a vicious circle in which low-income residences are built in areas devoid of green spaces and urban equipment (CEPAL, 2017). Other causes relate to the higher maintenance costs of urban vegetation, which have been related in different social contexts (Reyes-Päcke et al., 2014), (Byrne et al., 2016). Moreover, national research has determined that other factors, such as vandalism, device damage and the theft of irrigation equipment, can contribute to the lack of urban greenery in L_D in Chile (Reyes-Päcke et al., 2014).

Similarly, the increased building density in L_D often stems from unfair market dynamics (de Castro Mazarro et al., 2022), contributing to

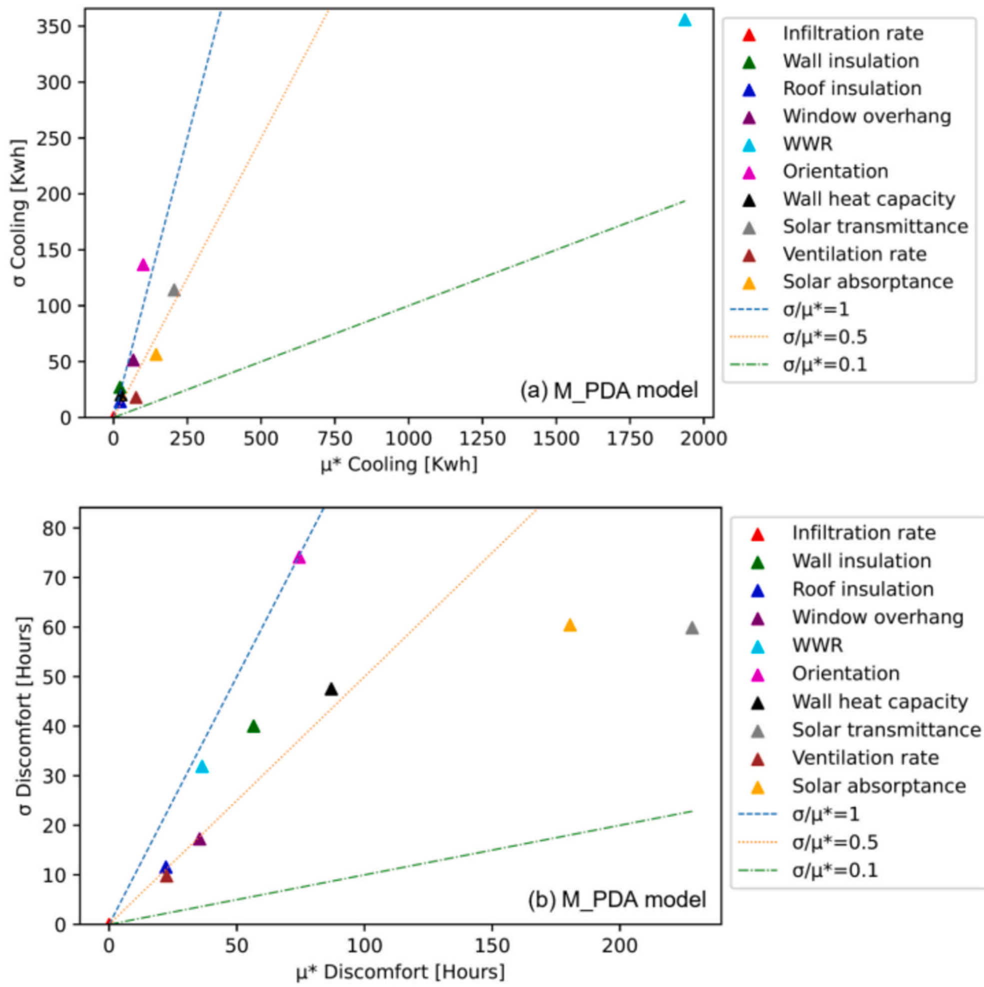

Fig. 15. Sensitivity analysis results in (a) M_PDA cooling loads and (b) M_PDA discomfort hours.

the rise of the UHII. In the case of Temuco, national indicators suggest that it is one of the cities experiencing significant ongoing urban development (INEb). This trend could exacerbate urban speculation and gentrification, leading to the displacement of poorer populations into suburbs with low urban design standards. This challenge is widespread in developing countries and has been observed in various Chilean cities, including Temuco (Sarricolea et al., 2022), (Rojo-Mendoza et al., 2019), (Vergara Erices, 2014).

Given this context, the UHI effect in L_D may be linked to factors such as the absence of urban vegetation and increased building density, which reduce soil permeability. The opposite is also true once poorer districts lead to disadvantageous UHI consequences. These issues signify a structural problem that necessitates resolution through public policies tailored to the unique characteristics of each urban zone and its socio-economic status. Addressing these challenges could help bridge the gaps between urban districts, alleviating the negative impacts of varied UHII within the same city. Moreover, although the diverse building performances observed in this research in different urban zones are not solely attributed to UHI, the consideration of urban influences in building design is crucial for formulating effective public policies. This idea applies either to statal strategies to mitigate urban inequalities or to the implementation of proper energy standards.

While it is true that colder cities experience a benefit in terms of energy heating expenses, in the evaluated city, it is difficult to balance the final cost and benefits of the UHI effect, considering that heating energy is almost covered for firewood fuel whilst cooling energy would be supported by electricity. Thus, considering a holistic analysis of energy sources, a life cycle assessment (LCA) and life cost assessment (LCC) could be interesting to better understand the final net balance and consequences of the triple bottom line. This type of analysis is quite important if socio-economic issues are considered, as electricity and firewood have very different budgets. According to official webpages on electricity bills in Chile (GCE) firewood local market prices (MMA, 2023), at the end of 2023, the electricity bill ($/kWh) is close to 400% higher than the equivalent caloric energy of firewood ($/kWh). This number is still conservative once other expenses charged to the final customer in the electricity supply are not considered in the calculations (GCE). Moreover, electricity production in Chile currently comprises 64.5% of non-renewable sources (ME, 2022). Thus, if the evaluated city becomes an electricity consumer for cooling purposes, another energy poverty issue will arise. Additionally, this problem tends to worsen if global warming and UHI are similarly considered (Verichev and Carpio, 2020).

Currently, energy poverty in southern South America, when referred to as the thermo-energy performance of homes, is discussed in terms of heating consumption (Calvo et al., 2021). However, studies highlighting how the UHI and/or global warming effect could be changing the historically known housing energy requirements regarding new energy poverty issues are scarce. In addition, current thermal codes could underestimate non-predominant climate conditions because they focus on just one concern. Thus, energy standards can be thoroughly reviewed to better adapt to new thermo-energy demands. Newer and more detailed analyses could define whether comparable thermal zones similar to Temuco could also be getting closer to new cooling energy consumption to include this requirement in public policies and social discussions. However, these transition processes should be carefully planned and addressed. Considering the complex dynamics involved in the use and engagement of new technologies or demands, a successful sustainable approach depends on institutional aspects as well as socio-technical practices developed on a domestic scale (Boso et al., 2017).

4.2. UHI and thermo-energy performance

Considering only residential neighbourhoods, UHII impacts on simulated buildings were not very different in varying LCZ classes, as mentioned above. However, it is worth discussing the disparities encountered in this and previous research. Although similar research where simulated UHI impact on residential buildings' energy performance in the same city is scarce, Zinzi and Carnielo (2017) and Zinzi et al. (2018) conducted comparable investigations (Zinzi and Carnielo, 2017), (Zinzi et al., 2018). The authors simulated residential models in Rome, Italy, and encountered an average UHII of 1.4 °C and percentual distinctions between urban and rural zones up to 46% in cooling energy demand in city centres and 12% in peripheral zones (Zinzi and Carnielo, 2017). Authors also reported urban–rural differences between 22% and 26% in cooling demands and 18%–24% in heating energy depending on the urban zone in Rome (Zinzi et al., 2018). Similarly, Palme et al. (2017) conducted research in four coastal cities in South America, simulating residential units in several urban zones (Palme et al., 2017). Although they customised urban parameters in every urban zone for modelling urban weather files, percentual energy demand differences between areas were lower (up to 14% depending on the city) than reported herein (up to 16%). Litardo et al. (2020) performed a similar investigation to Palme et al. (2017) in a tropical climate, where only cooling demand is needed. The authors found urban–rural differences in cooling demand between 30% and 70% in residential buildings depending on the urban zone, and variations between neighbourhoods kept around 20% (Litardo et al., 2020), which is similar to the maximums measured in this research.

Thus, according to the aforementioned research and current results, it would be possible to affirm that urban differences in building performance are approximately 0.1%–20%. As expected, special attention should be given to denser urban zones ($LCZ2_3$ class in Temuco), especially if they contain building uses that could suffer from UHII daily and nightly variations.

Importantly, a typical department had a huge impact on cooling energy loads, emphasising the relevance of the building type and the energy building parameters used. Furthermore, in this study, no floor insulation was incorporated into the building models, despite its recommendation for the climate zone in accordance with the newer energy standard requirements in Chile (MINVU, 2018a), (Actualización de Regulación Térmica, 2017) (MINVU, 2024). If floor isolation had been implemented, cooling loads would likely have been even higher. Similarly, thermal comfort adaptive results demonstrate how new requirements and thermal recommendations in Chile are designed specifically for colder seasons. This is easily observable in Fig. 11 when the model set with the previous standard (L_OGUC) performed better than the same model set with the newer one (L_PDA). This is even worse in M_FLAT, where discomfort hours are the highest. This happens in all the comfort models analysed. Once again, these results highlight the importance of considering the UHI effect and global warming in the design of effective energy standards.

4.3. Policy implications

Based on the results obtained in this research, several public policy strategies could be recommended to optimize urban planning. Firstly, urban morphological characterization combined with socioeconomic sectorization is a crucial approach when designing thermo-energy performance strategies for buildings. In Temuco, despite its medium-scale size, a differentiated UHII is observed across various urban areas, indicating that certain districts require more attention to reduce indices that trigger thermal inequalities, such as urban vegetation, building density, or anthropogenic heat from traffic. As demonstrated in Table 2, some indices show significant variation between urban districts, which could be strongly influenced by municipal regulations aimed at balancing these indices across the city. As expected, these disparities are also evident in residential buildings according to their socioeconomic status, representing a double-edged sword, as residential districts experience both overheating environments and buildings that are unprepared for such conditions.

In this context, the performance results of buildings highlight the disparities in their thermal properties and inherent characteristics across both analysed districts. This research demonstrates that buildings updated with new energy codes and located in low-income neighborhoods are more susceptible to overheating (Figs. 11 and 12), even when models in both districts are configured with the same parameters (Appendix A). These results are influenced by several factors, such as building size, which increases thermal loads per occupant, and building density, which reduces favourable conditions for natural ventilation.

Thus, public policies should be implemented to either improve building design and social behaviour according to urban location or to promote better urban amenities that enhance thermal performance (e.g. Urban parks). Similarly, disparities in results are notable when different building types are simulated. Figs. 9–11 illustrate how M_FLAT performed quite differently compared to single-family houses. Therefore, public policies should consider inherent architectural differences when designing energy codes. This is particularly crucial, for example, when new energy codes permit higher WWR, which can negatively impact the summer thermal performance of medium- and high-rise residential buildings.

Accordingly, sensitivity analyses conducted in this investigation showed that some passive design strategies could influence either cooling loads or thermal comfort conditions. This highlights the importance of in-depth analysis when unequal socio-economic factors that influence building performance are compared. Incorporating this type of analysis could serve as a powerful tool for defining specific regulations within energy codes that address new climatic urban demands. This is particularly crucial if the combination of UHI, global warming, and increasingly frequent heat waves persists, as it could lead to situations where L_D and its residents are unable to afford the energy required for cooling HVAC systems. Hence, as a main strategy, the passive design of housing stock should be prioritized. However, to successfully reach outcomes in this regard, public policies, including clear and detailed municipal ordinances, sustainable standards, technical guidance, urban instruction and other incentives, should be practised by local governments.

On the other hand, some technical approaches could be implemented and refined to better understand the real performance of buildings based on simulation engines. In this regard, the current study highlights (Fig. 7) the significance of ground temperature input parameters and their relevance to performance results. Field campaigns could be conducted to survey ground properties and thereby optimize simulation settings. Similarly, public surveys that gather valuable information about actual housing conditions—such as stove conditions, indoor temperatures, social thermal perception, and typical behaviour—could be employed to gain a deeper understanding of real residential conditions. The involvement of government institutions could help alleviate the social apprehension encountered in this research when collecting technical data.

4.4. Suggestions for future research

In this research, three semi-detached housing models were used to verify the reliability of the results. However, the typical department was not monitored. Future research could monitor indoor conditions in department samples with and without newer energy standards. Similarly, other non-residential building uses could be evaluated. Moreover, instead of only temperature, other parameters related to thermal comfort could be monitored (e.g. humidity or indoor wind velocity). Additionally, considering the importance of ground temperatures in final performance, the model results from the corresponding transferring of models into EnergyPlus could be validated through temperature sensors.

Other important research progress could be the consideration of urban contexts in the simulation process, which might be performed by urban energy modelling programs (e.g. CityBES, EnviMET or UMI). This will contribute to a better understanding of the socio-economic differences in the thermo-energy performance of residential buildings on a district or city scale. If sensitivity analyses were conducted, they could evaluate the heat emitted to urban air once it is known that strategies to maintain better indoor conditions could negatively affect the urban environment (Ulpiani, 2021).

Finally, the authors recommend extending and applying the approach of this research to other cities and climates, particularly in large urban centres where socio-economic disparities tend to be more pronounced. For this purpose, the direct participation of residents, as well as the involvement of official institutions responsible for housing quality and well-being, will be crucial. This broader approach is suggested to influence public policies, leading to the development of new strategies aimed at achieving more equitable and sustainable urban development.

5. Conclusion

Cities are facing urban overheating exacerbated by global warming, and within the same city, different UHII can be experienced based on urban inequalities and socioeconomic statuses. Considering this, the primary objective of this research was to address the following question: how do different urban zones, particularly residential buildings, experience the UHI effect in relation to their socio-economic status? To answer this question, the current study employs simulation analysis to examine the influence of the UHI effect on the thermo-energy performance of residential buildings. Additionally, this analysis is conducted based on the socio-economic status of the building models and urban zones within the evaluated city. Finally, to assess the importance of building parameters in thermo-energy performance, a sensitivity analysis was conducted on models with contrasting socio-economic levels. The following conclusions emerge from this investigation.

The UHI effect, the socioeconomic status of residential districts, and the thermo-energy performance of residential buildings are interconnected. Firstly, this connection is evident in how residential neighbourhoods are designed and configured in relation to the socioeconomic capacity to build and maintain urban indices (e.g., urban vegetation or building density). L_D demonstrated a lower capacity to mitigate urban overheating compared to M_D. Secondly, due to these disparities, residents in low-income districts tend to construct their homes with lower-quality materials, occupying more urban space at the expense of green or permeable areas, which are sacrificed for greater use of urban land. Furthermore, given Temuco's historically colder climate, residents often prepare their buildings with a focus on colder seasons, overlooking new demands related to the UHI effect and global warming. Lastly, this trend is exacerbated by local energy standards that are primarily designed to maintain indoor warmth, leading to unintended daytime indoor overheating when buildings are retrofitted to meet these newer codes, as demonstrated in this research. Moreover, indoor overheating was even higher depending on building typology, as resulted in M_FLAT simulations.

Considering these results, there is a need to review energy codes that are designed to adapt buildings to a single predominant climate, especially in cities that have historically faced colder temperatures. This revision is particularly pertinent in cities where socio-economic segregation, driven by expanding urbanization and inadequately prepared municipal ordinances governing urban land distribution, is a frequent phenomenon. This issue becomes even more critical if residential districts begin to require HVAC cooling systems where they were previously unnecessary. First, the affordability of these technologies in L_D is lower, which could lead to a new energy poverty issue. Second, the use of HVAC systems could potentially exacerbate the UHI effect through increased heat emissions from buildings. Therefore, it is possible to assert that there is a cause-and-effect relationship between socio-economic status in urban zones and urban warming.

Even though the UHI effect might bring some benefits during winter, it is crucial to consider the overall balance of its consequences, especially when the district's affordability plays a significant role in determining the capacity for well-being and quality of life in thermal comfort goals. This concern becomes particularly important considering the global warming effect and the heat wave phenomenon, which seem more recurrent and are projected to be more frequent in upcoming decades (Krelling et al., 2023).

In quantitative terms, this research obtained a few results, which are summarised as follows:

Urban-rural cooling energy load differences range between 12.47% and 38.92% depending on LCZ class, residence model analysed or energy building standard applied. This percentage average is 25.7%, which is similar to the overall average of 23.2% reported in previous studies (Lopez-Guerrero et al., 2023).

Urban–rural heating energy load differences range between −20.47% and −81.95%, depending on the LCZ class, residence model analysed or energy building standard applied. This percentage average is −51.21% and is higher than the −18% reported by worldwide investigations (Li et al., 2019), (Lopez-Guerrero et al., 2023). However, it is remarkable to state that the normal impacts of UHI on heating loads are underexplored in similar research, resulting in a scarcity of data for comparison (López-Guerrero et al., 2022).

When the same housing models are hypothetically located in different urban zones, energy performance distinctions range between 18% and 24% for heating loads and approximately 10%–16% for cooling loads in semi-detached house models. The latter percentages are similar to those reported in previous research on different climates and urban scales (Palme et al., 2017), (Litardo et al., 2020), (Zinzi and Carnielo, 2017), (Zinzi et al., 2018).

Urban–rural variations in thermal comfort time vary from 0.5% to 100%, contingent on factors such as the residential model, LCZ class, thermal zone and comfort model analysed. For living rooms, this percentage in different LCZ classes averaged 23.1%, 5.5% and 6% for the Dear and Brager, CIBSE TM52 and ASRHAE 55 (2010) comfort models, respectively. Correspondingly, for bedroom space in the M_FLAT model, this average is 15.6%, 47.8% and 52.8%.

If contrasting socio-economic semi-detached housing models are considered, discomfort hours in living rooms are 56.2%, 76.5% and 50.2% higher in low-income households, considering the Dear and Brager, CIBSE TM52 and ASRHAE 55 (2010) comfort models, respectively.

All these results highlight the importance of considering urban microclimates in the creation of thermo-energy standards that are well adapted to current and future demands in cities. The detailed influence of UHI on the housing stock or other building uses should also be considered for public policy makers and city planners, especially if it is intended to decrease the gaps between contrasting socio-economic statuses. The authors of this research believe that this is the only way to create a fairer and more sustainable future for all urban residents.

CRediT authorship contribution statement

Rafael E. López-Guerrero: Writing – original draft, Software, Methodology, Investigation, Formal analysis, Conceptualization. **Konstantin Verichev:** Writing – original draft, Validation, Supervision, Investigation, Conceptualization. **Juan Pablo Cárdenas-Ramírez:**

Writing – review & editing, Visualization, Validation, Methodology. **Manuel Carpio:** Writing – original draft, Validation, Supervision, Project administration, Funding acquisition, Conceptualization.

Declaration of competing interest

The authors declare that they have no known competing financial interests or personal relationships that could have appeared to influence the work reported in this paper.

Acknowledgements

This work was funded by: ANID/Scholarship Program/DOCTORATE SCHOLARSHIPS CHILE/2020–21201032; ANID BASAL FB210015 CENAMAD; ANID FONDECYT 1201052; **BG23/00134;** Pontificia Universidad Católica de Chile through the 2024 International Sabbatical Support Competition of the Academic Vice-Rectorship; and partially supported by the Vice-Rectorade for Research, Development, and Artistic Creation at Universidad Austral de Chile.

Appendix A

Table S1
Simulation parameters in EnergyPlus.

OGUC			PDA (Low- and high-medium income)		
Parameter	Value	Reference	Parameter	Value	Reference
Rural climate file	EPW Temuco 2007–2021	(Lawrie et al.)	Rural climate file	EPW Temuco 2007–2021	(Lawrie et al.)
Wall U value (W/m^{2}K)	1.32	Ordenanza General de Urbanismo y Contrucciones (2007)	Wall U value (W/m^{2}K)	0.45	MMA (2015)
Roof U value (W/m^{2}K)	0.3	Ordenanza General de Urbanismo y Contrucciones (2007)	Roof U value (W/m^{2}K)	0.27	MMA (2015)
Window U value (W/m^{2}K)	5.8	Larrea-Sáez et al. (2023)	Window U value (W/m^{2}K)	2.8	(MINVU, 2018a), (Larrea-Sáez et al., 2023)
Occupation (people)	3	(INE, 2017)	Occupation (people)	3	(INE, 2017)
Occupation schedule (living room)	0–14 h = 0; 14–18 h = 0.5; 18–22 h = 1; 22–24 h = 0 (Whole year)	NBR 15575 (2021)	Occupation schedule (living room)	0–14 h = 0; 14–18 h = 0.5; 18–22 h = 1; 22–24 h = 0 (whole year)	NBR 15575 (2021)
Occupation schedule (rooms)	0–08 h = 1; 08–22 h = 0; 22–24 h = 1. (whole year)	NBR 15575 (2021)	Occupation schedule (rooms)	0–08 h = 1; 08–22 h = 0; 22–24 h = 1. (whole year)	NBR 15575 (2021)
Occupation schedule (kitchen)	0–07 h = 0; 07–08 h = 1; 08–12 h = 0; 12–13 h = 1, 13–17 h = 0, 17–18 h = 1, 18–24 h = 0 (whole year)	Typical in analysed districts	Occupation schedule (kitchen)	0–07 h = 0; 07–08 h = 1; 08–12 h = 0; 12–13 h = 1, 13–17 h = 0, 17–18 h = 1, 18–24 h = 0 (whole year)	Typical in analysed districts
Metabolic activity	98.4 W (day) - 82 W (night)	MINVU (2018a)	Metabolic activity	98.4 W (day) - 82 W (night)	MINVU (2018a)
Infiltration rate ACH	24.6 (50pa) 1.57 (4pa)*	CITEC and DECON (2014) (*) Conversion from 50pa to 4pa made by methodology proposed in DesignBuilder software manual (DesignBuilder, 2023)	Infiltration rate proposed by PDA standard	7 (50pa) 0.45 (4pa)*	MMA (2015) (*) Conversion from 50pa to 4pa made by methodology proposed in DesignBuilder software manual (DesignBuilder, 2023)
Infiltration rate ACH after verification adjustment (4pa) (See Section 2.5)	1.76		Infiltration rate ACH after verification adjustment (4pa) (See Section 2.5)	0.47	
Lighting loads in rooms (w/m^2)	5	NBR 15575 (2021)	Lighting loads in rooms (w/m^2)	5	NBR 15575 (2021)
Equipment loads (living and kitchen) (w)	120	NBR 15575 (2021)	Equipment loads (living and kitchen) (w)	120	NBR 15575 (2021)
Natural ventilation availability schedules in AFN model (rooms)	From 22 h to 8 h (December to March)	Typical in analysed districts	Natural ventilation availability schedules in AFN model (rooms)	From 22 h to 8 h (December to March)	Typical in analysed districts
Natural ventilation availability schedules in AFN model (living room)	From 8 h to 22 h (December to March)	Typical in analysed districts	Natural ventilation availability schedules in AFN model (living room)	From 8 h to 22 h (December to March)	Typical in analysed districts
WWR East facade (%)	25	Typical in analysed districts	WWR east facade (%)	30	(Actualización de Regulación Térmica, 2017) East/West max. 42% with U value ≤ 2.8
WWR North facade (%)	25	Typical in analysed districts	WWR north facade (%)	36	(Actualización de Regulación Térmica, 2017) façade North max. 73% with U value ≤ 2.8
Maximum AFN ventilation temperature setpoint schedule (°C)	25	MINVU (2018b)	Maximum AFN ventilation temperature setpoint schedule (°C)	25	MINVU (2018b)
Heating setpoint (°C)	20	CChC (2014)	Heating setpoint (°C)	20	CChC (2014)
Cooling setpoint (°C)	25	MINVU (2018b)	Cooling setpoint (°C)	25	MINVU (2018b)

Obs. WWR in M_FLAT: 42% east façade (living room), 38% east façade (room), 72% north façade (main room) (Actualización de Regulación Térmica, 2017).

Appendix B

Table S2
Simulation parameters tested in sensitivity analysis.

Parameter/Unit for parametrisation	Units	Range	Explanation
Infiltration rate/(ACH)	Air change per hour (ACH)	{0.2, 0.3, 0.4, 0.5, 0.6, 0.7, 0.8, 0.9, 1, 1.1, 1.2, 1.3, 1.4, 1.5}	Rate of unintentional air entry from outside through the imperfections of building envelope
Wall insulation/(m)	W/(m_2 K)	{0.02, 0.03, 0.04, 0.05, 0.06, 0.07, 0.08}	Wall thermal insulation thickness
Roof insulation/(m)	W/(m^2 K)	{0.09, 0.1, 0.11, 0.12, 0.13, 0.14}	Roof thermal insulation thickness
Window overhang projection ratio/(%)	M	{0.2, 0.4, 0.6, 0.8}	Horizontal shading device over windows
WWR/(%)	%	{25, 35, 45, 55, 65, 75}	Percentual of windows regarding walls
Orientation/(°)	°	{0, 45, 90, 135, 180, 225, 270, 315, 360}	Building layout orientation in relation to north axis
Wall type/(exterior wall heat capacity)	KJ/(m^2 K)	{60.9, 222.5}	Heat capacity of exterior walls. Note that two walls were proposed, one light and one heavy (with the same U value)
Window solar transmittance/(%)	%	{0, 0.2, 0.4, 0.6, 0.8}	Window solar transmittance at normal incidence averaged over the solar spectrum
Ventilation change/(ACH)	Air change per hour (ACH)	{1, 1.5, 2.0, 2.5, 3.0, 3.5, 4.0, 4.5, 5.0}	Infiltration rate through open windows and doors. This parameter was sensitised in the Zone Ventilation: Design Flow Rate object
Wall solar absorptance/%	%	{0.2, 0.3, 0.4, 0.5, 0.6, 0.7, 0.8, 0.9}	Fraction of incident solar radiation absorbed by external walls and roof. Note that albedo = solar absorbance minus 1 (for opaque materials)

Data availability

Data will be made available on request.

References

Actualización de Regulación Térmica, 2017. *MINVU*. Chile [Online]. Available: https://www.minvu.gob.cl/wp-content/uploads/2023/04/Estandar-higrotermico_ZT-FyG.pdf. (Accessed 24 October 2023).

Alonso, A., Calama-González, C.M., Suárez, R., León-Rodríguez, Á.L., Hernández-Valencia, M., 2022. Improving comfort conditions as an energy upgrade tool for housing stock: analysis of a house prototype. Energy for Sustainable Development 66, 209–221. https://doi.org/10.1016/j.esd.2021.12.009.

Andrea, S., et al., 2008. In: Global Sensitivity Analysis: the Primer.

Aparicio-Fernández, C., Vivancos, J.L., Cosar-Jorda, P., Buswell, R.A., 2019. Energy modelling and calibration of building simulations: a case study of a domestic building with natural ventilation. Energies 12 (17). https://doi.org/10.3390/en12173360.

ASHRAE, 2010. In: "Standard 55-2010 – Thermal Environmental Conditions for Human Occupancy (ANSI Approved," Atlanta.

ASHRAE, 2014. In: ASHRAE. United Stated of America: American Society of Heating, Ventilating, and Air Conditioning Engineers.

Aslam, A., Rana, I.A., 2022. The Use of Local Climate Zones in the Urban Environment: A Systematic Review of Data Sources, Methods, and Themes. Elsevier B.V. https://doi.org/10.1016/j.uclim.2022.101120

Asociación Española de Normalización y Certificación, 1994. Determinación de la densidad de un suelo: Método de la balanza hidrostática (UNE 103301:1994). AENOR.

Bazaz, A., et al., 2018. In: Summary for Urban Policymakers: what the IPCC Special Report on 1.5 C Means for Cities. https://doi.org/10.24943/SCPM.2018.

Bechtel, B., Alexander, P.J., Böhner, J., Ching, J., Conrad, O., 2015. Mapping local climate zones for a worldwide database of the form and function of cities. ISPRS Int. J. Geo-Inf. 4, 199–219. https://doi.org/10.3390/ijgi4010199.

Bechtel, B., et al., 2019. Generating WUDAPT Level 0 data – current status of production and evaluation. Urban Clim. 27, 24–45. https://doi.org/10.1016/j.uclim.2018.10.001.

Bigladder Software, "EnergyPlus web-based documentation," EnergyPlus Web-Based Documentation. Accessed: November. 7, 2023. [Online]. Available: https://bigladdersoftware.com/epx/docs/.

Boccalatte, A., Fossa, M., Gaillard, L., Menezo, C., 2020. Microclimate and urban morphology effects on building energy demand in different European cities. Energy Build. 224. https://doi.org/10.1016/j.enbuild.2020.110129.

Bockarjova, M., Botzen, W.J.W., van Schie, M.H., Koetse, M.J., 2020. Property price effects of green interventions in cities: a meta-analysis and implications for gentrification. Environ Sci Policy 112, 293–304. https://doi.org/10.1016/j.envsci.2020.06.024.

Boso, À., Ariztía, T., Fonseca, F., 2017. Usos, resistencias y aceptación de tecnologías energéticas emergentes en el hogar. El caso de la política de recambio de estufas en Temuco. Rev. Int. Sociol. 75 (4). https://doi.org/10.3989/ris.2017.75.4.17.04.

Bueno, B., Norford, L., Hidalgo, J., Pigeon, G., 2013. The urban weather generator. J Build Perform Simul 6 (4), 269–281. https://doi.org/10.1080/19401493.2012.718797.

Bueno, B., Roth, M., Norford, L., Li, R., 2014. Computationally efficient prediction of canopy level urban air temperature at the neighbourhood scale. Urban Clim. 9, 35–53. https://doi.org/10.1016/j.uclim.2014.05.005.

Byrne, J., et al., 2016. Could urban greening mitigate suburban thermal inequity?: the role of residents' dispositions and household practices. Environ. Res. Lett. 11 (9). https://doi.org/10.1088/1748-9326/11/9/095014.

Calvo, R., Álamos, N., Billi, M., Urquiza, A., Contreras Lisperguer, R., 2021. Desarrollo de indicadores de pobreza energética en América Latina y el Caribe' serie Recursos Naturales y Desarrollo, N° 207 (LC/TS.2021/104), Santiago [Online]. Available: www.cepal.org/apps.

Camarasa, C., et al., 2022. A rapid-assessment model on the potential of district energy: the case of Temuco in Chile. Energy and Built Environment. https://doi.org/10.1016/j.enbenv.2022.02.003.

CChC, 2014. Manual de Instalaciones Térmicas.

CDT, 2019. Informe final de usos de energía de los Hogares Chile 2018.

CEPAL, 2017. Desarrollo sostenible, urbanización y desigualdad en América Latina y el Caribe. Dinámicas y desafíos para el cambio estructural.

Chakraborty, T., Hsu, A., Manya, D., Sheriff, G., 2019. Disproportionately Higher Exposure to Urban Heat in Lower-Income Neighborhoods: A Multi-City Perspective. Institute of Physics Publishing. https://doi.org/10.1088/1748-9326/ab3b99.

Chan, C., Delina, L.L., 2023. Energy Poverty and beyond: the State, Contexts, and Trajectories of Energy Poverty Studies in Asia. Elsevier Ltd. https://doi.org/10.1016/j.erss.2023.103168

Chen, D., Wang, X., Thatcher, M., Barnett, G., Kachenko, A., Prince, R., 2014. Urban vegetation for reducing heat related mortality. Environmental Pollution 192, 275–284. https://doi.org/10.1016/j.envpol.2014.05.002.

Choi, K., et al., 2023. Review of Infiltration and Airflow Models in Building Energy Simulations for Providing Guidelines to Building Energy Modelers. Elsevier Ltd. https://doi.org/10.1016/j.rser.2023.113327

Chong, A., Gu, Y., Jia, H., 2021. Calibrating Building Energy Simulation Models: A Review of the Basics to Guide Future Work. Elsevier Ltd. https://doi.org/10.1016/j.enbuild.2021.111533

CIBSE, 2013. The Limits of Thermal Comfort : Avoiding Overheating in European Buildings, vol. 2013.

Citec, U.B.B., Decon, U.C., 2014. Manual de hermeticidad al aire de edificaciones. Universidad del Bío-Bío.

Climate data, "Climate Data." Accessed: April. 6, 2023. [Online]. Available: https://es.climate-data.org/america-del-sur/chile/ix-region-de-la-araucania/temuco-6152/.

Crawley, D.B., et al., 2001. EnergyPlus: creating a new-generation building energy simulation program. Energy Build. 33, 319–331.

Culver, L.C., 2017. In: Energy Poverty: what You Measure Matters.

da Silva, R.G.P., Lima, C.L., Saito, C.H., 2023a. Urban green spaces and social vulnerability in Brazilian metropolitan regions: towards environmental justice. Land Use Pol. 129, 1–12. https://doi.org/10.1016/j.landusepol.2023.106638.

da Silva, R.G.P., Lima, C.L., Saito, C.H., 2023b. Urban green spaces and social vulnerability in Brazilian metropolitan regions: towards environmental justice. Land Use Pol. 129 (Jun). https://doi.org/10.1016/j.landusepol.2023.106638.

Davenport G, A., Susan, C., Grimmond, B., Oke, T.R., 2000. Estimating the roughness of cities and sheltered country. American Meteorological Society. Available: https://www.researchgate.net/publication/224001525.

de Castro Mazarro, A., Sikder, S.K., Pedro, A.A., 2022. Spatializing inequality across residential built-up types: a relational geography of urban density in São Paulo, Brazil. Habitat Int. 119 (Jan). https://doi.org/10.1016/j.habitatint.2021.102472.

De Dear, R., Brager, G.S., 1997. Developing an adaptive model of thermal comfort and preference [Online]. Available: https://www.researchgate.net/publication/269097185.

DesignBuilder, 2023. DesignBuilder manual [Online]. Available: https://designbuilder.co.uk/helpv7.0/Content/Airtightness_Scheduled.htm (Accessed 17 July 2023).

Duan, S., Luo, Z., Yang, X., Li, Y., 2018. The impact of building operations on urban heat/cool islands under urban densification: a comparison between naturally-ventilated and air-conditioned buildings. Appl. Energy 235, 129–138. https://doi.org/10.1016/j.apenergy.2018.10.108.

EnergyPlus, "EnergyPlus," Engineering Reference. Accessed: October. 27, 2023. [Online]. Available: https://bigladdersoftware.com/epx/docs/22-2/engineering-reference/.

Enescu, D., 2017. A Review of Thermal Comfort Models and Indicators for Indoor Environments. Elsevier Ltd. https://doi.org/10.1016/j.rser.2017.05.175

Eugenio Pappalardo, S., Zanetti, C., Todeschi, V., 2023. Mapping urban heat islands and heat-related risk during heat waves from a climate justice perspective: a case study in the municipality of Padua (Italy) for inclusive adaptation policies. Landsc Urban Plan 238. https://doi.org/10.1016/j.landurbplan.2023.104831.

Feitosa, F.O., Batista, P., Marques, J.L., 2023. How to assess spatial injustice: distinguishing housing spatial inequalities through housing choice. Cities 140 (Sep). https://doi.org/10.1016/j.cities.2023.104422.

Fernández, I.C., Koplow-Villavicencio, T., Montoya-Tangarife, C., 2023. Urban environmental inequalities in Latin America: a scoping review. World Development Sustainability 2, 100055. https://doi.org/10.1016/j.wds.2023.100055.

Garcia Sanchez, D., Lacarrière, B., Musy, M., Bourges, B., 2014. Application of sensitivity analysis in building energy simulations: combining first- and second-order elementary effects methods. Energy Build. 68 (PART C), 741–750. https://doi.org/10.1016/j.enbuild.2012.08.048.

García-Lamarca, M., Anguelovski, I., Venner, K., 2022. In: Challenging the Financial Capture of Urban Greening. Nature Research. https://doi.org/10.1038/s41467-022-34942-x.

GCE, "Tarifa de Suministro Eléctrico a Precio de estabilización 2023 vigente desde el 1 de noviembre 2023," Tarifa de Suministro Eléctrico a Precio de estabilización 2023 vigente desde el 1 de noviembre 2023. Accessed: November. 16, 2023. [Online]. Available: https://www.cge.cl/informacion-comercial/tarifas-y-procesos-tarifarios/tarifa-de-suministro/.

Gholizadeh Touchaei, A., 2015. Characterizing the Effect of Increasing Albedo on Urban Meteorology and Air Quality in Cold Climates, a Case Study for Montreal. Concordia University.

Giridharan, R., Emmanuel, R., 2018. The impact of urban compactness , comfort strategies and energy consumption on tropical urban heat island intensity : a review. Sustain. Cities Soc. 40 (January), 677–687. https://doi.org/10.1016/j.scs.2018.01.024.

González, V., Ramos Ruiz, G., Fernández Bandera, C., 2022. Ground characterization of building energy models. Energy Build. 254, 1–11. https://doi.org/10.1016/j.enbuild.2021.111565.

Grimmond, C.S.B., 1992. The suburban energy balance: methodological considerations and results for a mid-latitude west coast city under winter and spring conditions. Int. J. Climatol. 12 (5), 481–497. https://doi.org/10.1002/joc.3370120506.

Guevara, Z., Mendoza-Tinoco, D., Silva, D., 2023. The theoretical peculiarities of energy poverty research: a systematic literature review. Energy Res Soc Sci 105, 103274. https://doi.org/10.1016/j.erss.2023.103274.

Han, Y., He, J., Liu, D., Zhao, H., Huang, J., 2023. Inequality in urban green provision: a comparative study of large cities throughout the world. Sustain. Cities Soc. 89 (Feb). https://doi.org/10.1016/j.scs.2022.104229.

He, B.J., Ding, L., Prasad, D., 2020. Relationships among local-scale urban morphology, urban ventilation, urban heat island and outdoor thermal comfort under sea breeze influence. Sustain. Cities Soc. 60 (April), 102289. https://doi.org/10.1016/j.scs.2020.102289.

Henríquez, C., Romero, H., 2019. In: Urban Climates in Latin America. https://doi.org/10.1007/978-3-319-97013-4.

Hong, T., Ferrando, M., Luo, X., Causone, F., 2020. Modeling and analysis of heat emissions from buildings to ambient air. Appl. Energy 277 (July), 115566. https://doi.org/10.1016/j.apenergy.2020.115566.

IEA, "Is cooling the future of heating?," Is Cooling the Future of Heating? Accessed: Sep. 25, 2023. [Online]. Available: https://www.iea.org/commentaries/is-cooling-the-future-of-heating.

INE, "Instituto Nacional de Estadística," Proyecciones de población. Accessed: March. 25, 2023. [Online]. Available: https://regiones.ine.cl/araucania/estadisticas-regionales/sociales/demografia-y-vitales/proyecciones-de-poblacion.

INE, "Sistema de Indicadores y Estándares de Desarrollo Urbano," Sistema de Indicadores y Estándares de Desarrollo Urbano. Accessed: November. 16, 2023. [Online]. Available: https://www.ine.gob.cl/herramientas/portal-de-mapas/siedu/.

INE. Instituto Nacional de Estadística [Online]. Available: https://regiones.ine.cl/araucania/estadisticas-regionales/economia/edificacion-y-construccion/permisos-de-edificacion. (Accessed 25 September 2021).

Kato-Huerta, J., Geneletti, D., 2022. Environmental justice implications of nature-based solutions in urban areas: a systematic review of approaches, indicators, and outcomes. Environ Sci Policy 138, 122–133. https://doi.org/10.1016/j.envsci.2022.07.034.

Kim, H., Woosnam, K.M., Kim, H., 2022. Urban gentrification, social vulnerability, and environmental (in) justice: perspectives from gentrifying metropolitan cities in Korea. Cities 122 (Mar). https://doi.org/10.1016/j.cities.2021.103514.

Koch, K., Ysebaert, T., Denys, S., Samson, R., 2020. Urban heat stress mitigation potential of green walls: a review. Urban For. Urban Green. 55 (September), 126843. https://doi.org/10.1016/j.ufug.2020.126843.

Krelling, A.F., Lamberts, R., Malik, J., Hong, T., 2023. A simulation framework for assessing thermally resilient buildings and communities. Build. Environ. 245 (Nov). https://doi.org/10.1016/j.buildenv.2023.110887.

Kronenberg, J., Łaszkiewicz, E., Andersson, E., Biernacka, M., 2023. Popular but exclusive: how can lower socio-economic status groups win access to urban green spaces? Geoforum 143 (Jul). https://doi.org/10.1016/j.geoforum.2023.103774.

Larrea-Sáez, L., Cuevas, C., Casas-Ledón, Y., 2023. Energy and environmental assessment of the chilean social housing: effect of insulation materials and climates. J. Clean. Prod. 392 (Mar). https://doi.org/10.1016/j.jclepro.2023.136234.

Laverge, J., Janssens, A., 2013. Optimization of design flow rates and component sizing for residential ventilation. Build. Environ. 65, 81–89. https://doi.org/10.1016/j.buildenv.2013.03.019.

Lawrie, K. Linda, Drury B, C., Org, ClimateOneBuilding. Development of global typical meteorological years (TMYx) [Online]. Available: https://climate.onebuilding.org/contact/default.html. (Accessed 24 October 2023).

Li, H., et al., 2018. Interaction between urban heat island and urban pollution island during summer in Berlin. Sci. Total Environ. 636, 818–828. https://doi.org/10.1016/j.scitotenv.2018.04.254.

Li, X., Zhou, Y., Yu, S., Jia, G., Li, H., Li, W., 2019. Urban heat island impacts on building energy consumption: a review of approaches and findings. Energy 174, 407–419. https://doi.org/10.1016/j.energy.2019.02.183.

Lin, J., Zhang, H., Chen, M., Wang, Q., 2023. Socioeconomic disparities in cooling and warming efficiencies of urban vegetation and impervious surfaces. Sustain. Cities Soc. 92. https://doi.org/10.1016/j.scs.2023.104464.

Lindberg, F., Grimmond, C.S.B., 2011. In: The Influence of Vegetation and Building Morphology on Shadow Patterns and Mean Radiant Temperatures in Urban Areas : Model Development and Evaluation, pp. 311–323. https://doi.org/10.1007/s00704-010-0382-8.

Litardo, J., et al., 2020. Urban Heat Island intensity and buildings' energy needs in Duran, Ecuador: simulation studies and proposal of mitigation strategies. Sustain. Cities Soc. 62 (July), 102387. https://doi.org/10.1016/j.scs.2020.102387.

López-Guerrero, R.E., Verichev, K., Moncada-Morales, G.A., Carpio, M., 2022. How do urban heat islands affect the thermo-energy performance of buildings? J. Clean. Prod. 373, 1–21. https://doi.org/10.1016/j.jclepro.2022.133713.

Lopez-Guerrero, R.E., Verichev, K., Carpio, M., 2023. How do urban form and socioeconomic differences affect the microclimate of a residential district?. In: XXVII Congreso Internacional De Dirección e Ingeniería De Proyectos.

Mao, J., Yang, J.H., Afshari, A., Norford, L.K., 2017. Global sensitivity analysis of an urban microclimate system under uncertainty: design and case study. Build. Environ. 124, 153–170. https://doi.org/10.1016/j.buildenv.2017.08.011.

Martilli, A., Krayenhoff, E.S., Nazarian, N., 2020. Is the Urban Heat Island intensity relevant for heat mitigation studies? Urban Clim. 31, 100541. https://doi.org/10.1016/j.uclim.2019.100541.

Mastrucci, A., Byers, E., Pachauri, S., Rao, N.D., 2019. Improving the SDG energy poverty targets: residential cooling needs in the Global South. Energy Build. 186, 405–415. https://doi.org/10.1016/j.enbuild.2019.01.015.

Matos, A.M., Delgado, J.M.P.Q., Guimarães, A.S., 2022. Linking Energy Poverty with Thermal Building Regulations and Energy Efficiency Policies in Portugal. MDPI. https://doi.org/10.3390/en15010329.

Matzarakis, A., Wetterdienst, D., Rutz, F., Matzarakis, A., Rutz, F., 2006. RayMan: a tool for research and education in applied climatology. In: 8 Th Conference on Meteorology-Climatology-Atmospheric Physics Athens [Online]. Available: https://www.researchgate.net/publication/233759055.

Maucec, D., Premrov, M., Leskovar, V.Z., 2021. Use of sensitivity analysis for a determination of dominant design parameters affecting energy efficiency of timber buildings in different climates. Energy for Sustainable Development 63, 86–102. https://doi.org/10.1016/j.esd.2021.06.003.

ME, 2022. Informe Balance Nacional de Energía 2020.

Meteochile. Dirección Meteorológica de Chile [Online]. Available: http://www.meteochile.gob.cl/PortalDMC-web/index.xhtml. (Accessed 27 March 2023).

MINVU, 2018a. "Estandares de Construccion Sustentable para Viviendas en Chile, Tomo II: Energia," Santiago [Online]. Available: https://csustentable.minvu.gob.cl/estandares-cs/. (Accessed 10 May 2024).

Ministerio de Vivienda y Urbanismo, 1999. Ordenanza General de Urbanismo y Construcciones (Decreto Supremo N.º 47). Ministerio de Vivienda y Urbanismo, Santiago, Chile.

MINVU, 2018b. Estándares de construcción sustentable para viviendas de Chile - Tomo I: Salud y Bienestar.

MINVU, 2019. Manual De Procedimientos Calificación Energética De Viviendas En Chile.

MINVU. Chile: Ministerio de Vivienda y Urbanismo, 2024.

MMA, "Mejoramiento térmico de viviendas," Mejoramiento térmico de viviendas. Accessed: August. 25, 2023. [Online]. Available: https://airearaucania.mma.gob.cl/mejoramiento-termico-de-viviendas/.

MMA, 2015. Chile [Online]. Available: https://www.leychile.cl/N?i=1084085&f=2015-11-17&p=. (Accessed 24 October 2023).

MMA, 2023. Reporte de Leña Región de la Araucanía [Online]. Available: Reporte de lena y pellets mes de Noviembre https://mma.gob.cl/araucania/reporte-de-lena-region-de-la-araucania/. (Accessed 16 November 2023).

Montaner-Fernández, D., et al., 2020. Spatio-temporal variation of the urban heat island in Santiago, Chile during summers 2005–2017. Remote Sens (Basel) 12 (20), 1–19. https://doi.org/10.3390/rs12203345.

Morris, M.D., 1991. In: American Society for Quality Factorial Sampling Plans for Preliminary Computational Experiments.

Nakano, A., Bueno, B., Norford, L., Reinhart, C.F., 2015. Urban weather generator user interface development: new workflow for integrating urban heat island effect in urban design process. In: ICUC9 -9thInternational Conference on Urban Climate Jointly with12thSymposium on the Urban Environment [Online]. Available: http://urbanmicroclimate.scripts.mit.edu.

NBR 15575-1, ABNT. Brasil, 2021.

Netatmo, "Netatmo." Accessed: March. 28, 2023. [Online]. Available: https://www.netatmo.com/.

Ogando, A., Cid, N., Fernández, M., 2017. Energy modelling and automated calibrations of ancient building simulations: a case study of a school in the northwest of Spain. Energies 10 (6). https://doi.org/10.3390/en10060807.

Oke, T.R., 1995. The Heat Island of the Urban Boundary Layer: Characteristics, Causes and Effects. Wind Climate in Cities, pp. 81–102. https://doi.org/10.1007/978-94-017-3686-2.

Oke, T.R., 2006. In: Initial Guidance to Obtain Representative Meteorological Observations at Urban Sites.

Oke, T.R., Mills, G., Christen, A., Voogt, J.A., 2017. Urban Climates. First publ. Cambridge University Press.

ONU, 2018. World Urbanization Prospects, vol. 12 [Online]. Available: https://population.un.org/wup/publications/Files/WUP2018-Report.pdf.

Ordenanza General de Urbanismo y Contrucciones, 2007. Ministerio de Vivienda y Urbanismo, Chile. https://www.minvu.gob.cl/elementos-tecnicos/circulares-division-de-desarrollo-urbano-ddu/de-la-arquitectura-condiciones-de-habitabilidad-4-1-1-al-4-1-16/. (Accessed 10 May 2024).

Palme, M., Inostroza, L., Villacreses, G., Lobato-Cordero, A., Carrasco, C., 2017. From urban climate to energy consumption. Enhancing building performance simulation by including the urban heat island effect. Energy Build. 145, 107–120. https://doi.org/10.1016/j.enbuild.2017.03.069.

Peel, M.C., Finlayson, B.L., Mcmahon, T.A., 2007. Updated world map of the Köppen-Geiger climate classification. Hydrol. Earth Syst. Sci. 11 (5), 1633–1644.

Pérez-Fargallo, A., A, P.A.J., Rubio-Bellidob, C., Trebilcockc, M., Pideritb, B., Attia, S., 2018. Development of a new adaptive comfort model for low income housing in the central-south of Chile. Energy Build. 178. https://doi.org/10.1016/j.enbuild.2018.08.030.

Quah, A.K.L., Roth, M., 2012. Diurnal and weekly variation of anthropogenic heat emissions in a tropical city , Singapore. Atmos. Environ. 46, 92–103. https://doi.org/10.1016/j.atmosenv.2011.10.015.

Reyes, R., Sanhueza, R., Schueftan, A., 2020. Consumo de leña y otros biocombustibles sólidos en la región de la Araucanía: nuevas cifras y tendencias [Online]. Available: www.infor.cl.

Reyes-Päcke, S., De, F., Barrera, L.A., Dobbs, C., Spotorno, A., Pavez, C., 2014. Costos de manutención de las áreas verdes urbanas en Chile - Informe final.

Rojo-Mendoza, F., Jara-Rojas, T., Frick-Raggi, J.P., 2019. Gated communities in the intermediate city. The Case of Temuco (Chile), 2005-2014. Universidad Nacional de Colombia. https://doi.org/10.15446/bitacora.v29n1.63192.

Roy J., P., et al., 2018. Sustainable Development, Poverty Eradication and Reducing Inequalities. In: global Warming of 1.5°C. An IPCC Special Report on the impacts of global warming of 1.5°C above pre-industrial levels and related global greenhouse gas emission pathways. In the Context of Strengthening the Global Response to the Threat of Climate Change, Sustainable Development, and Efforts to Eradicate Poverty [Online]. Available: https://www.ipcc.ch/report/sr15/chapter-5-sustainable-development-poverty-eradication-and-reducing-inequalities/.

Salvati, A., Monti, P., Coch Roura, H., Cecere, C., 2019. Climatic performance of urban textures: analysis tools for a Mediterranean urban context. Energy Build. 185, 162–179. https://doi.org/10.1016/j.enbuild.2018.12.024.

Santamouris, M., 2014. On the energy impact of urban heat island and global warming on buildings. Energy Build. 82, 100–113. https://doi.org/10.1016/j.enbuild.2014.07.022.

Santamouris, M., Fiorito, F., 2021. On the impact of modified urban albedo on ambient temperature and heat related mortality. Sol. Energy 216 (November 2020), 493–507. https://doi.org/10.1016/j.solener.2021.01.031.

Santamouris, M., Cartalis, C., Synnefa, A., Kolokotsa, D., 2015. On the impact of urban heat island and global warming on the power demand and electricity consumption of buildings - a review. Energy Build. 98, 119–124. https://doi.org/10.1016/j.enbuild.2014.09.052.

Sarricolea, P., Meseguer-Ruiz, O., 2019. Urban climates of large cities: comparison of the urban heat Island effect in Latin America. In: Urban Climates in Latin America. Springer International Publishing, pp. 17–32. https://doi.org/10.1007/978-3-319-97013-4_2.

Sarricolea, P., Smith, P., Romero-Aravena, H., Serrano-Notivoli, R., Fuentealba, M., Meseguer-Ruiz, O., 2022. Socioeconomic inequalities and the surface heat island distribution in Santiago, Chile. Sci. Total Environ. 832 (October 2021), 155152. https://doi.org/10.1016/j.scitotenv.2022.155152.

SECTRA. Programa de Vialidad y Transporte urbano [Online]. Available: https://www.sectra.gob.cl/. (Accessed 19 April 2022).

Stewart, I.D., Oke, T.R., 2012. Local climate zones for urban temperature studies. Bull. Am. Meteorol. Soc. 93 (12), 1879–1900. https://doi.org/10.1175/BAMS-D-11-00019.1.

Tammaru, T., Marcińczak, S., Aunap, R., van Ham, M., Janssen, H., 2020. Relationship between income inequality and residential segregation of socioeconomic groups. Reg. Stud. 54 (4), 450–461. https://doi.org/10.1080/00343404.2018.1540035.

Temuco, 2015. Estudio de paisaje e imagen urbana. Temuco [Online]. Available: https://legacy.temuco.cl/wp-content/uploads/2018/12/Cap5-Imagen-Urbana.pdf. (Accessed 27 March 2023).

Ulpiani, G., 2021. On the linkage between urban heat island and urban pollution island: three-decade literature review towards a conceptual framework. Sci. Total Environ. 751, 141727. https://doi.org/10.1016/j.scitotenv.2020.141727.

UN. The 17 sustainable development goals (SDGs) [Online]. Available: https://sdgs.un.org/goals. (Accessed 9 November 2019).

UN-HABITAT, 2012. State of Latin American and Caribbean Cities 2012 towards a New Urban Transition. Kenia [Online]. Available: (Accessed 11 April 2023).

UNEP, 2020. Global Status Report for Buildings and Construction: towards a Zero-Emission, Efficient and Resilient Buildings and Construction Sector [Online]. Available: https://wedocs.unep.org/bitstream/handle/20.500.11822/34572/GSR_ES.pdf?sequence=3&isAllowed=y.

Vanessa Aparecida, C.D.C., Karin Maria, S.C., 2017. Manual Do Pré-Processador Slab. Sao Carlos [Online]. Available:

Venter, Z.S., Figari, H., Krange, O., Gundersen, V., 2023. Environmental justice in a very green city: spatial inequality in exposure tourban nature, air pollution and heat in Oslo, Norway. Sci. Total Environ. 858 (Feb). https://doi.org/10.1016/j.scitotenv.2022.160193.

Vergara Erices, L.A., 2014. El Estado subsidiario y sus políticas urbanas: la expulsión de los estratos bajos de la ciudad. GeoGraphos. Revista Digital para Estudiantes de Geografía y Ciencias Sociales 5. https://doi.org/10.14198/geogra2014.5.62.

Verichev, K., Carpio, M., 2020. Effects of climate change on variations in climatic zones and heating energy consumption of residential buildings in the southern Chile. Energy Build. 215, 109874. https://doi.org/10.1016/j.enbuild.2020.109874.

Wagner, M., Viswanathan, V., 2016. Analyzing the impact of driving behavior at traffic lights on urban heat. Procedia Eng. 169, 303–307. https://doi.org/10.1016/j.proeng.2016.10.037.

WHO, 2009. In: International Society of City and Regional Planners (ISOCARP).

Woong Kim, S., Brown, R.D., 2021. Urban heat island (UHI) intensity and magnitude estimations: a systematic literature review. Sci. Total Environ. 779. https://doi.org/10.1016/j.scitotenv.2021.146389.

Yang, S., Tian, W., Cubi, E., Meng, Q., Liu, Y., Wei, L., 2016. Comparison of sensitivity analysis methods in building energy assessment. In: Procedia Engineering. Elsevier Ltd, pp. 174–181. https://doi.org/10.1016/j.proeng.2016.06.369.

Yang, X., Li, Y., Luo, Z., Chan, P.W., 2017. The urban cool island phenomenon in a high-rise high-density city and its mechanisms. Int. J. Climatol. 37 (2), 890–904. https://doi.org/10.1002/joc.4747.

Yang, X., et al., 2020. Impact of urban heat island on energy demand in buildings: local climate zones in Nanjing. Appl. Energy 260 (30), 114279. https://doi.org/10.1016/j.apenergy.2019.114279.

Zhang, Y., Jankovic, L., 2017. JEA, an interactive optimisation engine for building energy performance simulation. In: *Building Simulation Conference Proceedings*, International Building Performance Simulation Association, pp. 1923–1932. https://doi.org/10.26868/25222708.2017.607.

Zhang, R., Zhang, C.Q., Cheng, W., Lai, P.C., Schüz, B., 2021. The neighborhood socioeconomic inequalities in urban parks in a High-density City: an environmental justice perspective. Landsc Urban Plan 211 (Jul). https://doi.org/10.1016/j.landurbplan.2021.104099.

Zinzi, M., Carnielo, E., 2017. Impact of urban temperatures on energy performance and thermal comfort in residential buildings. The case of Rome, Italy. Energy Build. 157, 20–29. https://doi.org/10.1016/j.enbuild.2017.05.021.

Zinzi, M., Carnielo, E., Mattoni, B., 2018. On the relation between urban climate and energy performance of buildings. A three-years experience in Rome, Italy. Appl. Energy 221 (April), 148–160. https://doi.org/10.1016/j.apenergy.2018.03.192.

Zuhaib, S., Hajdukiewicz, M., Goggins, J., 2019. Application of a staged automated calibration methodology to a partially-retrofitted university building energy model. J. Build. Eng. 26 (Nov). https://doi.org/10.1016/j.jobe.2019.100866.